ISSN 1075-7015, Geology of Ore Deposits, 2018, Vol. 60, No. 3, pp. 241–264. © Pleiades Publishing, Ltd., 2018.
Original Russian Text © B.B. Damdinov, L.B. Damdinova, 2018, published in Geologiya Rudnykh Mestorozhdenii, 2018, Vol. 60, No. 3, pp. 274–300.

Zun-Ospa Gold Deposit, Eastern Sayan: Geology, Ore Composition, and Genesis

B. B. Damdinov[a], * and L. B. Damdinova[a]

[a]*Geological Institute, Siberian Branch, Russian Academy of Sciences, Ulan-Ude, 670047 Russia*

**e-mail: damdinov@mail.ru*

Received October 25, 2015

Abstract—The paper discusses the geology of Zun-Ospa gold deposit, which is situated near the Ospino ophiolitic nappe in the southeastern part of the Eastern Sayan, and the ore composition therein. The deposit is related to the tectonic mélange zone and is characterized by distinct structural control. Three consecutive mineral assemblages formed within a temperature range of 380°–170°C: (i) native gold–quartz–pyrite, (ii) gold–quartz–polysulfide, and (iii) silver–sulfosalt. The ore was deposited from low-concentration (5.2–14.2 wt % NaCl equiv.) solutions without CO_2, with the predominance of Mg and Fe chlorides and an admixture of Na and K chlorides. The major ore minerals are pyrite, chalcopyrite, galena, and sphalerite; identified subordinate minerals are pyrrhotite, pentlandite, heazlewoodite, fahlore (tennantite, freibergite), Ni and Ag sulfosalts (ullmannite, miargyrite, polybasite, stephanite), Ag sulfides (mckinstryite, argentite); Au minerals are represented by electrum, kuestelite, and native gold of medium to low fineness. The geological, mineralogical, geochemical, and isotopic characteristics of ore indicate a metamorphic–hydrothermal genesis of mineralization related to the formation of a mélange zone in the duplex strike-slip structure. The sources of ore components are host rock complexes that have been subjected to tectonic deformations, among which rocks of an ophiolitic association predominate, along with fragments of initial hydrothermal–sedimentary ore, granitic, terrigenous, and carbonate rocks. The Late Paleozoic (352 Ma) age of mineralization corresponds to the stage of postcollision shear deformations within the entire Central Asian Foldbelt.

Keywords: Southeastern part of Eastern Sayan, Zun-Ospa gold deposit, mélange, mineralogy, geochemistry, metamorphic–hydrothermal genesis

DOI: 10.1134/S1075701518030029

INTRODUCTION

Various types objects differing in formation conditions and ore composition are known among gold deposits localized in southeastern part of the Eastern Sayan. The question on the their genesis remains incompletely solved. In some cases, genetic or paragenetic links with granitic bodies have been more or less reliably recorded (the Konevinskoe, Tainsky, etc., deposits). Some deposits are referred to polygenetic objects, e.g., the Zun-Kholba deposit, or are related to near-surface hydrothermal systems (Southern, Green, Dynamite deposits) (Airiyants et al., 2007; Damdinov et al., 2016; Gordienko et al., 2016; Mironov et al., 2001; Mironov and Zhmodik, 1999). At the same time, the genetic nature of certain deposits remains ambiguous. The Zun-Ospa deposit discovered by V.V. Levitsky in 1961 is one of them. Prospecting and geological exploration were carried out at this deposit in the 1960s and 1990s century; they continue intermittently to this day. The composition and genesis of this deposit are not covered in the literature except for sporadic mention in several publications: (Gordienko et al. 2016; Mironov and Zhmodik, 1999; *Zoloto Buryatii*, 2000). The Zun-Ospa gold deposit is medium-sized in total reserves; however, it remains insufficiently explored at depth and on its flanks. From the metallogenic aspect, the deposit is related to the Ospino ore cluster, which is an eastern continuation of the Urik–Kitoi gold ore zone (Mironov and Zhmodik, 1999).

The aim of our study is to establish the geological position of the Zun-Ospa gold deposit and ore composition therein to gain insight into its origin. The following sections address solutions to particular problems.

RESEARCH METHODS

During fieldworks at the deposit, we carried out geological observations of relationships between ore and host rocks, accompanied by sampling.

The chemical compositions of rocks and ores, including contents of trace elements, Au, and Ag, were determined by chemical analysis, atomic absorption, X-ray fluorescence, and spectral methods at the Geological Institute, Siberian Branch, Russian Academy

of Sciences (analysts B.Zh. Zhalsaraev, A.A. Tsyrenova, and others). The sulfur and oxygen isotopic compositions were determined at the Far East Geological Institute, Far East Branch, Russian Academy of Sciences (analyst T.A. Velivetskaya) and the Geological Institute, Siberian Branch, Russian Academy of Sciences (analyst V.F. Posokhov).

Petrographic study was performed using Olympus BX51 and Polam P-312 optical microscopes. The chemical compositions of ore minerals were studied at the Geological Institute, Siberian Branch, Russian Academy of Sciences on a Leo-1430 SEM with a quantitative Inca-Energy EDS attachment (analysts S.V. Kanakin and E.A. Khromova; parts of analyses have been borrowed from (unpublished data by Poselenov et al., 2012)).

Geochronological studies were carried out by U–Pb dating of zircons at the Geological Institute, Siberian Branch, Russian Academy of Sciences (analysts V.B. Khubanov and M.D. Buyantuev) and by Ar/Ar dating of muscovite at the Institute of Geology and Mineralogy, Siberian Branch, Russian Academy of Sciences (analysts A.V. Travin and D.S. Yudin). For the applied analytical technique, see (Travin et al., 2009; Khubanov et al., 2016).

For thermobarogeochemical studies of fluid inclusions (FIs) in mineral-forming media, the conventional thermo- and cryometric method was used, with a Linkam THMSG-600 microthermostage with a temperature measurement range from –196 to +600°C with LinkSys-32 software, at the Geological Institute, Siberian Branch, Russian Academy of Sciences. The total salinity (NaCl equiv.) of solution was determined from cryometric data according to (Bodnar and Vityk, 1994).

GEOLOGY OF THE DEPOSIT

The main macrostructural units in southeastern part of the Eastern Sayan in the nearest environment of the Zun-Ospa gold deposit are the Gargan Block, a jut of the crystalline basement of the Archean Tuva–Mongolian paleomicrocontinent with the retained Neoproterozoic carbonate platform cover (Irkut Formation) obducted over this structure, as well as ophiolites and neoautochthonous terrigenous rocks (*Geologiya i rudonosnost'* ..., 1989; Gordienko et al., 2016). The age of ophiolites is estimated within an interval greater than 1000–800 Ma (Kuz'michev and Larionov, 2013; Khain et al., 2002). All these complexes are cut through by intrusive bodies (mainly granitic) differing in age and genesis.

The deposit is located in marginal part of a granitic pluton close to western end of the Ospino ophiolitic nappe (Ospino–Kitoi ultramafic massif) among rocks of a mélange nappe, which includes sedimentary rocks of the Ilchir Sequence, the Ospino Formation, a mafic–ultramafic ophiolitic complex, and granitic rocks of the intrusive Sumsunur complex (Fig. 1). The central part of deposit is covered by Neogene olivine basalt.

The Ilchir Sequence mainly consists of black carbonaceous–micaceous–cherty, carbonaceous–clayey–carbonate, carbonaceous–carbonate–cherty, and quartz–amphibole–micaceous rocks with interbeds of carbonaceous limestone and marlstone, grayish green metavolcanics, and quartz-bearing fine-grained sandstone. Greenish gray micaceous–chlorite–carbonate, chlorite–actinolite, and quartz–chlorite schists occur in subordinate amounts. In the upper part of the sequence, mélange and olistostrome units with olistoliths of the Irkut Formation (limestone and dolomite) and of an ophiolitic association (ultramafic rocks serpentinized to various degrees) are prevalent. Contacts with the underlying Irkut Formation are tectonic everywhere (unpiblished data by Skopintsev et al., 2013).

The Ospino Formation is a terrigenous volcanic component of an ophiolitic association. The formation is composed of metagabbro, metabasic rocks, and tephroids metamorphosed under greenschist facies conditions of regional metamorphism; the upper sequence consists of limestone and black shale with layers of basic volcanic rocks and oligomictic sandstone (unpublished data by Kulikov et al., 1999).

Ultramafic rocks in the area of the deposit have been transformed into serpentinite, listvenite, and talc–carbonate rocks; initial rocks are absent. Serpentinite occurs in the Ospino–Kitoi ultramafic massif (nappe), which bounds the ore field of the deposit in the southeast, whereas in zones of tectonites, ultramafic rocks have been converted into listvenite, making up boudins and talc–carbonate rocks, as a mélange matrix. The basic rocks have been altered under action of secondary processes and metamorphism with transformation into quartz–sericite–epidote–chlorite propylite and mylonite, as well as chloritolith. Unaltered varieties of basic rocks have not been recorded.

Granitic rocks are related to the *Sumsunur Complex*, which is a representative example of the tonalite–trondhjemite–granodiorite (TTG) series, the age of which is estimated at 790 Ma (Kuz'michev, 2004). The most abundant are greenish gray medium-grained granitic rocks. The rocks are mainly composed of plagioclase (40–60%) sericitized to various degrees, quartz (10–25%) making up irregular isometric segregations, and dark-colored minerals (10–15%): hornblende and biotite; the latter is commonly acutely dominant. Potassium feldspar is represented by sporadic lattice microcline. Dark minerals are replaced with chlorite, tremolite, and epidote. Accessory minerals are magnetite, apatite, zircon, allanite, and less frequently, titanite and xenotime. The SiO_2 contents in rocks vary from 59.1 to 65.8 wt %; this value corresponds to quartz diorite and granodiorite (Table 1).

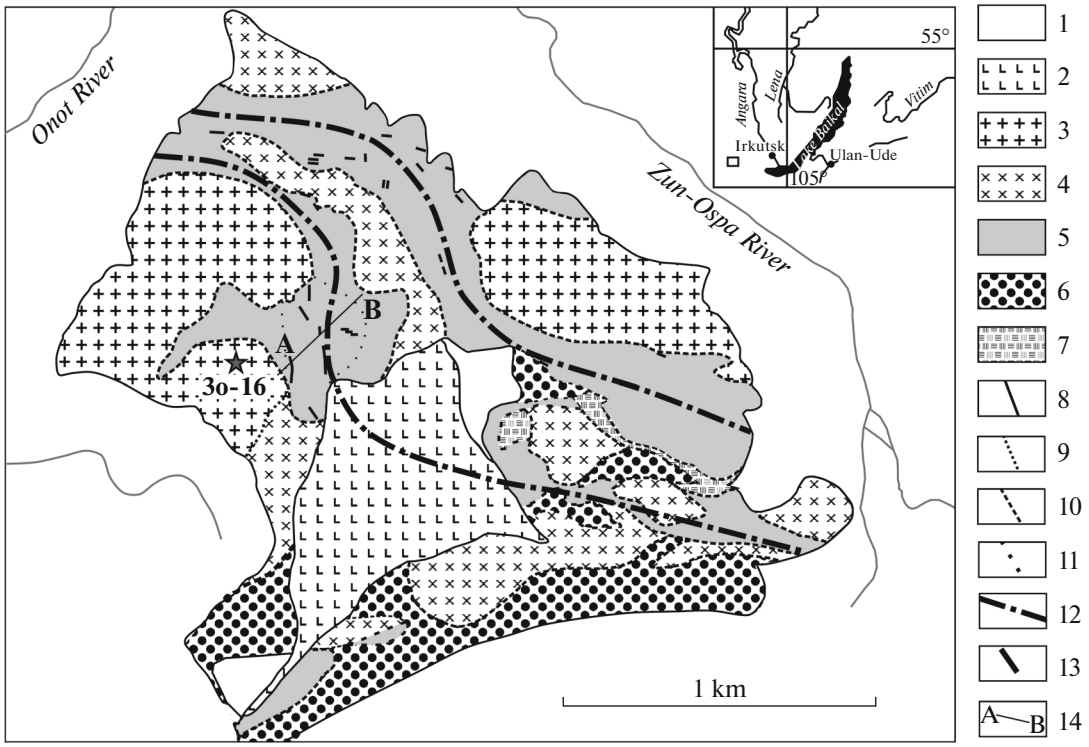

Fig. 1. Schematic geological map of central part of Zun-Ospa gold deposit. Compiled after data of (unpublished data by Kulikov et al., 1999). (1) Contemporary sediments unspecified; (2) Neogene basalt; (3) plagiogranite and granodiorite; (4) diorite and gabbrodiorite; (5) tectonites in mélange zones unspecified; (6) serpentinite mélange (sole of ophiolitic nappe); (7) talc–carbonate rock; (8) boundary between rocks different in age; (9) facies transition; (10) boundary of tectonic zone; (11) contour of ore zone no. 1; (12) general strike of axial part in mélange zone; (13) quartz and quartz–sulfide veins (out of scale); (14) line of geological section shown in Fig. 3; starlet indicates place of granite sampling for U–Pb dating (sample Zo-16).

The rocks are of sodic specialization; the Na/K ratios vary from 1.22 to 2.96. Minimum values are characteristic of intensely mylonitized granitic rocks enriched in sericite. The rocks are characterized by relatively low contents of incompatible elements. U–Pb dating of zircons has yields an age of 788.2 ± 7.1 Ma, which agrees with the earlier determined age of granitic rocks pertaining to the Sumsunur Complex (Fig. 2, Table 2). In addition, altered gabbronorite of the first phase of the Sumsunur Complex occurs at the deposit in a small quantity.

The majority of igneous rocks have been subjected to mylonitization and cataclasis, expressed in the development of oriented crosscutting stringerlike fine-grained aggregates quartz–epidote–zoisite–sericite in composition; oriented quartz, plagioclase, and dark-colored minerals; and enrichment in sericite, chlorite, and quartz up to the formation of carbonate–chlorite–quartz–sericite, carbonate–quartz–sericite, quartz–chlorite, and tremolite–chlorite–quartz–sericite blastomylonites occasionally containing rare plagioclase relics.

The basis of the structural and geologic position of the deposit is represented by a massif of granitic rocks broken into blocks, which are bounded by mélange zones with a mainly northwestern strike (Fig. 1). The central block is an intrusive dome composed of apical and deep-seated granitic rock facies. The maximum concentration of ore veins and zones is related to strike-slip duplexes at the flexure of the mélange structure.

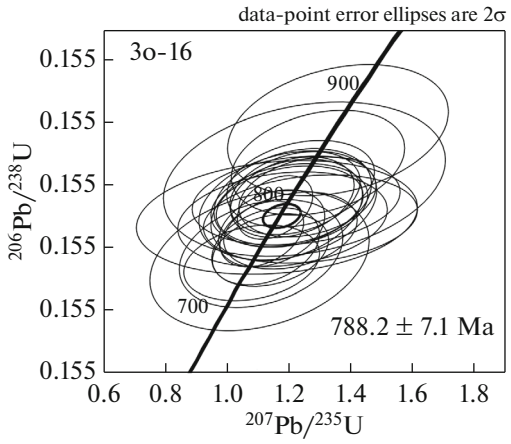

Fig. 2. Results of U–Pb dating of zircons from granitic rocks.

Table 1. Chemical composition of granitic rocks

Sample	zo-229	zo-240	zo-244	zo-260	zo-261	zo-28	zo-37
SiO_2	62.30	64.10	64.00	65.80	59.10	64.00	63.50
TiO_2	0.56	0.49	0.47	0.41	0.50	0.46	0.49
Al_2O_3	15.70	15.90	15.80	16.50	15.60	15.70	15.10
Fe_2O_3	2.34	0.95	0.88	1.67	0.97	1.20	2.04
FeO	3.88	3.38	3.56	2.32	4.60	3.27	2.97
MnO	0.10	0.07	0.07	0.06	0.10	0.05	0.09
MgO	2.33	1.60	1.80	1.52	2.25	1.80	1.83
CaO	5.19	2.85	2.75	4.19	4.95	2.80	3.64
Na_2O	3.82	3.92	3.69	3.19	2.87	4.21	3.80
K_2O	1.29	2.65	2.55	1.84	2.36	1.91	2.59
P_2O_5	0.18	0.16	0.18	0.14	0.18	0.13	0.12
LOI	2.21	4.25	4.50	2.14	6.50	4.12	3.35
Total	99.90	100.32	100.25	99.78	99.98	99.65	99.52
Ba	410	1150	850	770	860	810	880
Rb	24	48	44	29	40	26	55
Sr	430	200	204	390	325	190	340
Nb	5	4	4	5	3	6	5
Zr	120	124	94	81	69	74	137
Y	14	9	9	9	14	15	16
Cr	173	63	150	530	133	88	111
Ni	34	15	18	17	20	16	19
Co	17	12	12	10	17	10	14
V	118	74	73	59	112	75	95
Cu	76	26	12		20	0	18
Pb	32	19	36	10	130	7	17
Zn	38	43	215	32	52	55	43
Sn	2						
Mo	5						2
La	16	25	31	26	24	22	24
Ce	34	41	45	42	42	30	41
Na/K	**2.96**	**1.48**	**1.45**	**1.73**	**1.22**	**2.2**	**1.47**

The mélange that divides the granitic blocks is autoclastic and consists of tectonites after the aforementioned rock complexes. Four varieties of mélange have been selected.

The basis of mélange 1 is composed of beresite- and propylite-like tectonites, blocks of carbonate rocks, schists, and epi-serpentinite tectonites (listvenites). The blocks are small, and their contribution to the mélange volume is insignificant (1–2%).

Mélange 2 consists of the same rocks, but differs in block size (up to 40 m across) and mélange volume (up to 10–20%). Blocks composed of several petrographic varieties are known.

Mélange 3 is polymictic; altered granitic rocks, serpentinite, listvenite, limestone, quartzite, basic rocks, etc., occur therein. The matrix of tectonites is film- and ribbon-type and occupies 10–20% of the mélange body.

Mélange 4 is composed of talc–carbonate and hematite–talc–carbonate rocks; altered granitic rocks dominate in blocks.

In fact, all varieties of tectonized metasomatic rocks are close to one another in composition and differ only in their proportions in blocks (boudins) and the host matrix.

The three most abundant varieties are: (1) epi-ultramafic listvenite and talc–carbonate rocks con-

Table 2. Results of U–Pb isotopic dating of zircons from granite (sample Zo-16) in ore field of Zun-Ospa deposit by LA-ICP-MS

No.	Pb^{207}/U^{235}	1σ	Pb^{206}/U^{238}	1σ	Rho	Pb^{207}/U^{235} age	1σ	Pb^{206}/U^{238} age	1σ	D
1	1.214	0.0809	0.133	0.0026	0.298	**807**	37.08	**804.9**	15.05	0.2609
2	1.3599	0.1447	0.1437	0.0043	0.28	**871.8**	62.24	**865.7**	24.14	0.7046
3	1.2256	0.1367	0.1325	0.0029	0.1956	**812.4**	62.35	**802**	16.46	1.2968
4	1.1957	0.0994	0.131	0.0033	0.3049	**798.6**	45.98	**793.3**	18.9	0.6681
5	1.1135	0.1071	0.124	0.0035	0.2961	**759.9**	51.43	**753.7**	20.22	0.8226
6	1.2057	0.0964	0.1317	0.0026	0.247	**803.2**	44.36	**797.7**	14.82	0.6895
7	1.2221	0.0858	0.1336	0.0027	0.2887	**810.7**	39.22	**808.6**	15.39	0.2597
8	1.296	0.114	0.1385	0.0034	0.2816	**844**	50.39	**836.3**	19.43	0.9207
9	1.1639	0.1839	0.1298	0.0037	0.1814	**783.8**	86.31	**786.6**	21.23	–0.356
10	1.2395	0.0971	0.1352	0.0028	0.2682	**818.6**	44.02	**817.2**	16.1	0.1713
11	1.1574	0.0493	0.1314	0.0021	0.3682	**780.7**	23.2	**795.9**	11.72	–1.91
12	1.1998	0.1167	0.1317	0.0036	0.2794	**800.5**	53.87	**797.6**	20.41	0.3636
13	1.2145	0.1035	0.1329	0.0032	0.2854	**807.2**	47.44	**804.1**	18.4	0.3855
14	1.2526	0.1848	0.1359	0.005	0.2515	**824.6**	83.29	**821.3**	28.58	0.4018
15	1.0829	0.0886	0.1226	0.0025	0.2474	**745.1**	43.17	**745.3**	14.26	–0.027
16	1.108	0.1439	0.1229	0.0046	0.2869	**757.2**	69.34	**747.2**	26.28	1.3383
17	1.1816	0.1377	0.1295	0.0031	0.2048	**792**	64.07	**784.9**	17.65	0.9046
18	1.1274	0.0703	0.1252	0.0025	0.3229	**766.5**	33.55	**760.4**	14.43	0.8022
19	1.1427	0.0763	0.1245	0.0024	0.285	**773.8**	36.16	**756.6**	13.59	2.2733
20	1.1474	0.0695	0.128	0.0025	0.3249	**776**	32.87	**776.5**	14.4	–0.064
21	1.2717	0.1406	0.1295	0.0029	0.2004	**833.1**	62.85	**785.2**	16.4	6.1004
22	1.2072	0.0875	0.1277	0.0025	0.2722	**803.9**	40.26	**774.8**	14.38	3.7558
23	1.1146	0.0548	0.1272	0.0022	0.3456	**760.4**	26.31	**771.6**	12.38	–1.452
24	1.203	0.1029	0.1318	0.0027	0.2404	**802**	47.43	**798**	15.43	0.5013
25	1.2615	0.09	0.1331	0.0026	0.2738	**828.6**	40.42	**805.3**	14.81	2.8933

1σ, standard deviation; Rho, coefficient of standard deviation correlation; D, discordance, %.

sisting of quartz, magnesian carbonates, and talc with admixture of chlorite, fuchsite, sericite, and pyrite, frequently silicified; (2) beresite-like tectonites after granitic rocks representing quartz–sericite, carbonate–quartz–sericite, frequently silicified rocks with various proportions of quartz and sericite with an oriented structure; (3) propylite-like tectonites after basic rocks characterized by green color owing to the occurrence of such minerals as chlorite and epidote, although quartz and sericite occur as well; an oriented structure is also characteristic. These rocks correspond to their protoliths in compositions, differing only by an elevated potassium content.

In the south, the deposit is bounded by a serpentinite mélange zone, which frames (underlies) a nappe of ultramafic rocks in the Ospino–Kitoi massif. Hypsometrically, the upper part of the deposit is overlapped by a cover of Neogene–Quaternary olivine basalt with an ancient weathering mantle at the sole. The basaltic cover overlies the central part of the ore field. It should be noted that no dikes are mentioned within the ore field.

The ore-hosting structures are zones of tectonized and mineralized metasomatic rocks (Fig. 1). The Main, Northern, and Southern ore zones are traced beyond the area of the deposit, making up a horsetail structure. The total extent of ore zones is 9 km. The economic grades have been revealed in the vertical interval of 2000–2600 m. The Main Zone is the most promising.

In general view, the structure of the Main ore zone is as follows: a relatively simple slightly branching zone of mineralized tectonites or a cluster of two to three interweaved zones is traced for the entire extent. In the central segment of the ore zone, its structure becomes more complicated: in addition to main orebody no. 1, there is a series of smaller mineralized zones. The visible thickness of the tectonic zones varies from 200 to

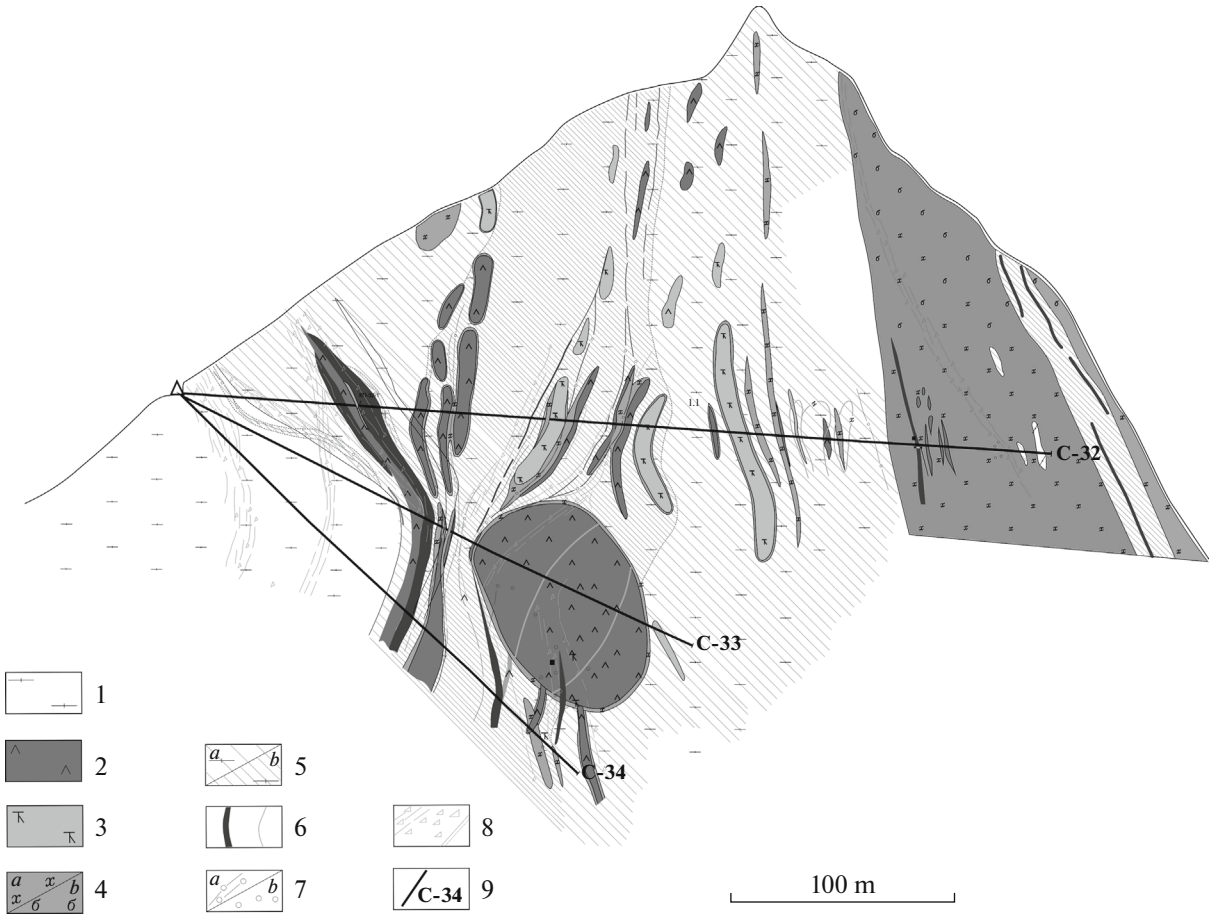

Fig. 3. Geological section along line A–B. Compiled after data of OOO S/A Kitoi (unpublished data by Poselenov, 2012). (1) Altered cataclastic granitic rocks; (2) quartz–carbonate and carbonate–quartz listvenites; (3) talc–carbonate and carbonate–talc rocks, talcite; (4) tectonized propylite-like metasomatic rocks: (*a*) quartz–carbonate–chlorite, (*b*) quartz–carbonate–biotite; (5) tectonized beresite-like metasomatic rocks: (*a*) carbonate–sericite–chlorite–quartz, (*b*) chlorite–sericite–quartz and sericite–quartz; (6) quartz veins and veinlets; (7) silicification: (*a*) stringer, (*b*) lenticular–pocket; (8) zones of crushing and brecciation, tectonic sutures with clay gouge; (9) borehole projection and its number.

600 m. The strike of the ore zone is nearly meridional, caused by bending of the near-latitudinal strike-slip structure.

Orebodies are represented by sulfide–quartz veins with silicified selvages and lenticular boudinlike quartz–sulfide bodies, where quartz and sulfide contents vary from massive sulfide ore to quartz–sulfide aggregates with equal amounts of quartz and ore minerals and low-sulfide quartz veins containing separate ore pockets. The vein zones are controlled by tectonic zones and do not go beyond these boundaries (Fig. 3). The dip and strike of veins are compatible with the attitude of tectonites. The upper units of the deposit consist of oxidized ore composed mainly of quartz–limonite and quartz–hematite–limonite aggregates containing malachite and azurite. Native gold, kuestelite, native silver, argentite, and other minerals of noble metals concentrate in the oxidized zone, which is not considered in this paper.

We have studied the largest and high-grade ore zone no. 1 (Ananino), which is a quartz–sulfide body with a central quartz-vein zone near the Neogene basalt cover. The quartz–sulfide body consists of a series of boudins traced for 50 m; the thickness of the body reaches 8 m across. Quartz veins are up to 0.8 m in thickness and traced for a distance up to 10–15 m. The veined quartz is a fine- to medium-grained mosaic aggregate with rare chlorite, sericite, and carbonates. The veins are framed by selvages of silicified rocks composed of inequigranular quartz with an allotriomorphic-granular microstructure, although some of the veins are devoid of distinct outer selvages and are immediately incorporated into tectonites after various rocks, where only thin (less than 1 cm) splays and bedding-plane sulfide–quartz stringers are noted. The low-sulfide veins are often clustered into stringer–disseminated zones up to a few meters thick.

The age of ore is determined by Ar/Ar dating of Cr-muscovite (fuchsite) from tectonized listvenite. This

age corresponds to the Early Carboniferous (352.3 Ma) (Fig. 4). As is seen, the age of ore is very distinct from the age of granitic rocks (Sumsunur Complex) in the ore field.

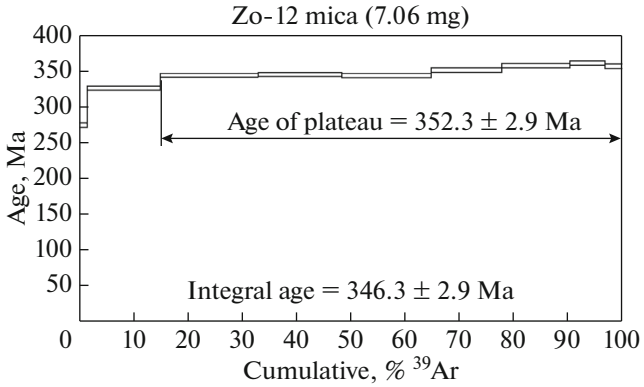

Fig. 4. Ar/Ar age of plateau for mica from tectonized listvenite at vein contact.

ORE MINERALOGY

Two main morphological types of gold mineralization are distinguished in the Zun-Ospa deposit: (1) low-sulfide quartz veins with silicified selvages and (2) quartz–polysulfide mineralized zones (ore boudins). Sites primarily composed of pyrite or chalcopyrite–pyrite–sphalerite–galena are distinguished in the latter. The zones of sulfide disseminations and quartz stringers in tectonites and metasomatic rocks are devoid of high-grade gold mineralization.

Ore-bearing quartz is macroscopically fine-grained, gray, white, and less milky white in color. Two quartz varieties are distinguished under an optical microscope. (1) Coarse-grained quartz makes up veins with relatively low ore mineral contents. Coarse (up to 5–7 mm) quartz grains are isometric in shape and with smoothed edges. A distinctly expressed wavy extinction emphasizes the cataclastic microstructure. Coarse quartz segregations are, as a rule, intensely fractured, and fractures are sealed with an aggregate of fine quartz grains (10–30 μm in dimensions). (2) Another variety of quartz is fine-grained (0.1–0.2 mm) aggregate with occasionally rare coarse grains, which are isometric and with tortuous jagged edges, and wavy extinction. Such quartz makes up the quartz–polysulfide mineralized zones.

Ores are characterized by relatively simple phase compositions with predominant minerals of a gold–polysulfide assemblage: pyrite, chalcopyrite, galena, sphalerite. The identified subordinate minerals are pyrrhotite, pentlandite, heazlewoodite, fahlore (tennantite, freibergite), Ni and Ag sulfosalts (ullmannite, miargyrite), Ag sulfides (polybasite, mckinstryite, stephanite, argentite), native gold, kuestelite, and native silver. The representative chemical compositions of ore minerals are given in Table 3.

The most abundant ore mineral is *pyrite,* which occurs as euhedral or subhedral crystals and aggregates of irregular isometric grains (Fig. 5a). Pyrite ore makes up mineralized zones of silicification with a stringer–disseminated character of ore mineral distribution or quartz–pyrite veins and veinlets with pockets of monomineralic pyrite aggregate. The structural etching of pyrite aggregates indicates the presence of two generations of pyrite. Pyrite-1 is known as rounded or irregular relict grains in pyrite-2 within monomineralic quartz–pyrite veins and veinlets; it does not contain sulfide microinclusions (Fig. 5b). In polysulfide ore, pyrite-2 is frequently corroded by aggregates of galena, sphalerite, and chalcopyrite up to the formation of skeletal grains or it contains numerous inclusions of the aforementioned sulfides (Figs. 5c, 5d). Owing to the high detection limit, the chemical composition data reveal no difference between pyrites related to various generations.

Galena and sphalerite make up joint aggregates with different proportions of these minerals. Sphalerite grains have a rounded isometric shape and are always more isomorphic than galena grains. The latter make up allotriomorphic-granular aggregates or fill interstices between sphalerite segregations (Fig. 6a). However, such indications as even boundaries, lack of corrosion tracks, or replacement of sphalerite allow us to assert that both minerals crystallize synchronously. The higher idiomorphism of sphalerite with respect to galena is explained by its higher capability for crystallization. Galena is characterized by its stoichiometric chemical composition, and no admixtures are identified at the level of analysis sensitivity (a few tenths of a percent). Sphalerite is ferriferous (up to 6.45 wt % Fe); in addition, it contains Cd (up to1.45 wt %) and emulsion impregnations and stringerlike segregations of chalcopyrite.

Chalcopyrite occurs as two generations: chalcopyrite-1 makes up joint aggregates with galena and sphalerite, stringers, selvages, and inclusions in pyrite-2, as well as emulsion impregnation in sphalerite (Fig. 6b). Chalcopyrite-2 makes up independent aggregates with relics of galena and sphalerite or corrodes galena–sphalerite intergrowths in the form of selvages (Fig. 6c).

Pyrrhotite together with *pentlandite* and *heazlewoodite* occurs sporadically and makes up rounded intergrowths within aggregates of chalcopyrite-2. These minerals are not identified separately from chalcopyrite-2 (Fig. 5d).

Fahlores are represented by tennantite (As up to 15.67 wt %, Ag up to 3.31 wt %, and freibergite (Sb up to 23.28 wt %, Ag up to 29.52 wt %). These minerals are identified as fine crystalline inclusions in pyrite and chalcopyrite grains, as well as in interstices between minerals of polysulfide assemblage: galena, sphalerite, chalcopyrite, and pyrite (Fig. 5b).

Table 3. Representative chemical compositions of ore minerals from Zun-Ospa deposit

Sample	Mineral	Fe	Co	Ni	Cu	Zn	Ag	Cd	Pb	Sb	As	S	Total
30_225	Chalcopyrite	31.02			34.02							35.44	100.48
30_225	Chalcopyrite	31.27			33.89							34.90	100.06
30_210	Chalcopyrite	31.44			33.16							35.51	100.11
30_225	Galena								88.61			12.52	101.13
30_225	Pyrite	47.44										53.40	100.84
30_210	Pyrite	47.50										52.59	100.08
30_210	Tennantite	6.20			37.89	3.81	3.31			5.57	15.26	27.85	99.89
30_210	Tennantite	6.28			38.5	3.68	3.03			6.01	15.67	27.81	100.98
30_225	Freibergite	9.19			15.47	0.85	29.52			23.28		22.37	100.68
30_225	Ullmannite	3.50		24.06	3.58					50.67		17.87	99.68
30_225	Ullmannite	0.62	0.48	26.29						58.73		15.33	101.45
30_225	Sphalerite	6.24				58.75		1.45				33.71	100.15
30_225	Sphalerite	6.45				58.88		0.80				33.51	99.64
1*	Stephanite						70.83			15.80		13.37	100
2*	Polybasite				2.95		73.67			10.92		12.46	100
3*	Argentite (acanthite)						83.67					16.33	100
4*	Mckinstryite				11.24		70.31		3.55			14.90	100
5*	Heazlewoodite	2.07		72.43								25.50	100
6*	Pentlandite	18.66		45.69								35.65	100

Chemical composition of minerals, according to (unpiblished data by Poselenov et al., 2012). Analyses were carried out at Geological Institute, Siberian Branch, Russian Academy of Sciences, on a Leo-1430 SEM with Inca-Energy EDS attachment (analysts S.V. Kanakin and E.A. Khromova).

According to the data of our forerunners (unpublished data by Kulikov et al., 1999; Poselenov et al., 2012), *sulfoantimonides and silver sulfides* occur in ore. These are polybasite $[Ag_9CuS_4][(Ag,Cu)_6(Sb,As)_2S_7]$, mckinstryite $(Ag,Cu)_2S$, stephanite Ag_5SbS_4, and argentite (acanthite) Ag_2S, which make up complex aggregates as rims and selvages around galena and chalcopyrite. Some of the listed minerals obviously formed in the oxidation zone, because such minerals as polybasite, acanthite, and mckinstryite occur in selvages, also containing secondary Pb, Zn, and Cu minerals (anglesite, cerussite, covellite). However, some of the Ag-bearing sulfosalts occur as inclusions and intergrowths with primary sulfides, and this indicates their hypogenic origin (Fig. 7a). Segregations of sulfosalts and Ag-bearing minerals are, as a rule, thin; their sizes do not exceed 10–20 μm. They are mainly related to interstices between major ore minerals or are identified as fine inclusions in the latter.

Ni and Ag sulfoantimonides (ullmannite and miargyrite) have been discovered as myrmekite-like intergrowths within interstices between galena and chalcopyrite grains (Fig. 7b). In addition, a mineral phase recalculated to the formula $Fe_2(Cu,Ag)_2S_4$ has been identified as an irregular elongated inclusion in pyrite (Figs. 7c, 7d).

Thus, three consecutive mineral assemblages have been established in ore of the Zun-Ospa deposit (Fig. 8): (i) **quartz–pyrite** (quartz, pyrite-1), (ii) **quartz–polysulfide** (pyrite-2, galena, sphalerite, chalcopyrite-1, chalcopyrite-2, pyrrhotite, pentlandite, heazlewoodite), and (iii) **Ag-sulfosalt** (fahlores, Ni and Ag sulfoantimonides, Ag sulfides, native silver). The minerals of the Ag-sulfosalt assemblage occur in minor amounts in primary ore, and some of them formed due to supergene transformation of ore. Nevertheless, some minerals related to the Ag-sulfosalt assemblage are contained in the primary ore.

Gold minerals. During gravitational separation of native gold grains from comminuted samples, oxidized quartz–hematite ore turns out to be the highest-grade. Gold grains have also been selected from low-sulfide quartz veins and quartz–polysulfide ore. According to grain-size composition, native gold is fine. Gold grains vary in dimensions from 0.1 to 0.9 mm.

Native gold is represented by isometric subhedral crystals, as well as elongated or rounded isometric grains with smoothed edges. Native gold is mostly

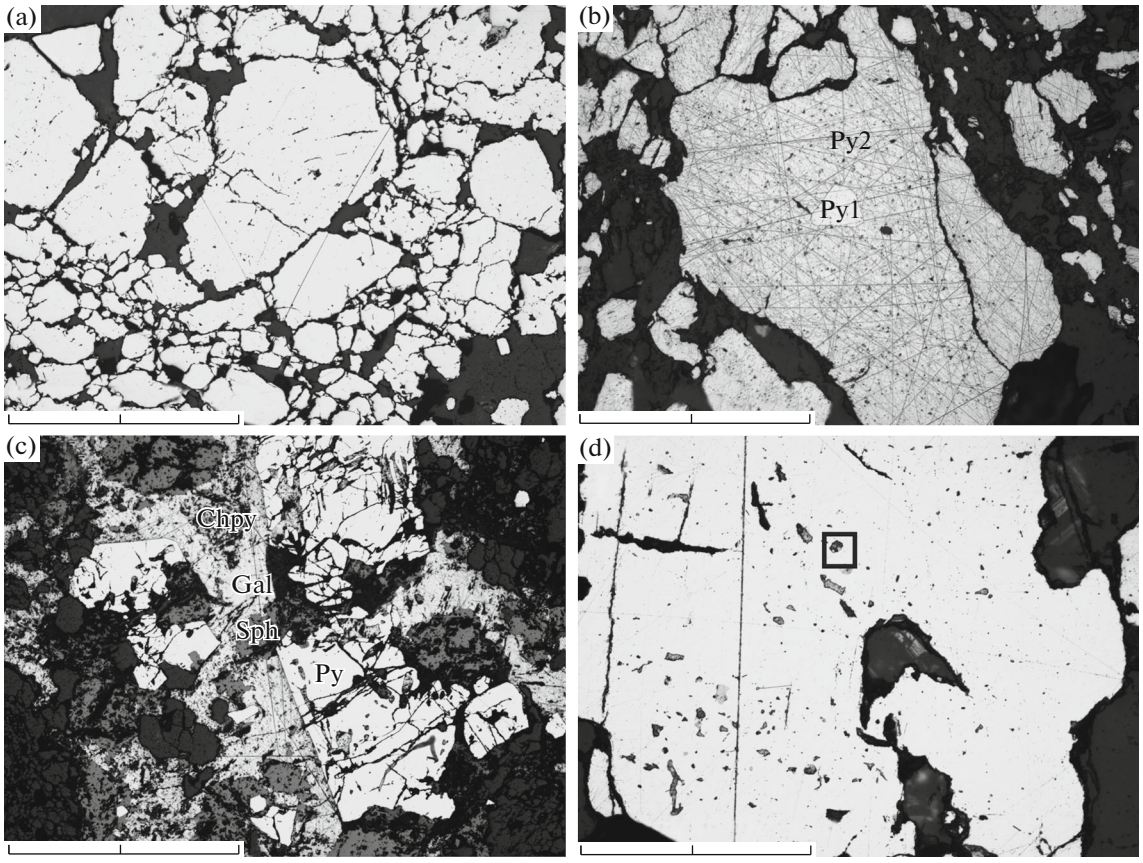

Fig. 5. Photomicrographs of pyrite segregations: (a) microstructure of pyrite ore; (b) relics of pyrite-1 in pyrite-2 grains; (c) skeletal crystals of pyrite-2 replaced with chalcopyrite–sphalerite–galena aggregate; (d) pyrite-2 crystal with numerous inclusions of minerals from polysulfide assemblage; polymineral gold–galena–sphalerite–chalcopyrite inclusion is shown in frame. Py, pyrite; Chpy, chalcopyrite; Gal, galena. Length of scale ruler is 500 μm.

associated with minerals of quartz–pyrite and quartz–polysulfide assemblages. Rounded gold inclusions occur directly in pyrite (Fig. 9a). Although gold is more frequently related to galena aggregates or incorporated in polymineral inclusions in pyrite-2 composed of galena, sphalerite, and chalcopyrite-1, gold also occurs directly in quartz (Figs. 9b, 9d).

The observed relationships between gold, ore, and gangue minerals show that kuestelite and electrum are incorporated into quartz–pyrite and quartz–polysulfide assemblages, whereas high-fineness gold is obviously later and associated with minerals of the Ag-sulfosalt assemblage, where they also occurs as rims, stringers, and inclusions in grains of kuestelite and electrum (Fig. 9c)

The chemical compositions of native gold are summarized in Table 4; a histogram of the fineness distribution is shown in Fig. 10. The general scatter of native gold fineness is estimated as from 194 to 854‰, i.e., from Au-bearing silver (kuestelite) to medium-fineness native gold.

Quartz–polysulfide ore is characterized by the lowest gold fineness (194–443 ‰); values in the range of 350–450‰ are predominant. The average fineness value is 357‰ with a rather large dispersion (the standard deviation is 94) and asymmetry toward lesser values; coefficient of asymmetry is –0.84. In low-sulfide quartz veins gold is distinguished in general by elevated fineness values from 444 to 852‰; the maximum falls on 450–500‰ (electrum), the average value is 531‰ with a standard deviation of 151 and asymmetry toward higher values (the asymmetry coefficient is 1.38). The statistic parameters of the gold fineness distribution in oxidized ore are close to those in quartz veins. The common scatter of fineness is 444–854‰ with an average value of 585‰; the standard deviation is 142; asymmetry is toward greater values; the asymmetry coefficient is 0.88.

CHEMICAL COMPOSITION OF ORE

The chemical composition of ore comprises Cu (0.86 wt %, on average), Pb (2.11 wt %, on average), Zn (1.77 wt %, on average), and Fe (7.14 wt %, on average) (Table 5). Depending on the relationships between the main ore-forming minerals—pyrite, galena, sphalerite, and chalcopyrite—the concentra-

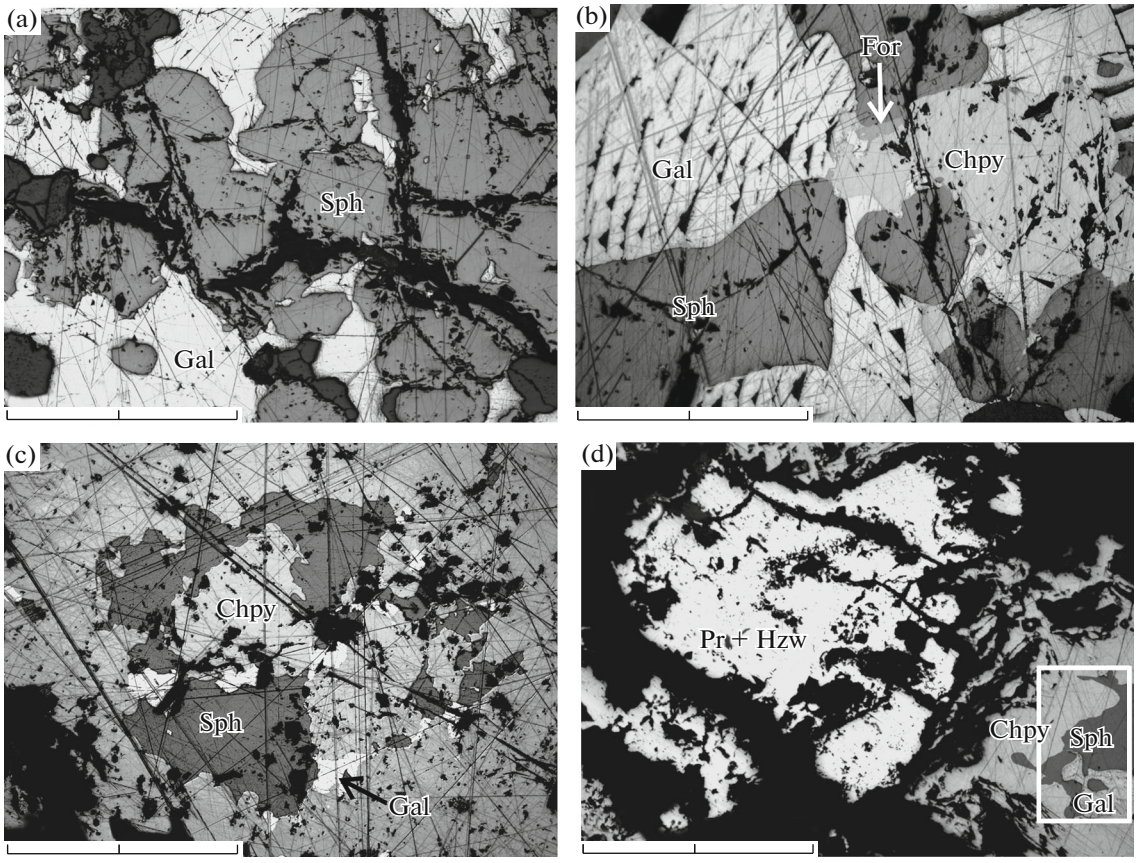

Fig. 6. Minerals of polysulfide assemblage: (a) galena–sphalerite aggregate; (b) chalcopyrite-1–galena–sphalerite aggregate; small segregations of fahlore in interstices; (c) relics of galena–sphalerite aggregate in chacopyrite-2; (d) aggregate of pyrrhotite and heazlewoodite intergrown with chalcopyrite-2; a relic of galena–sphalerite aggregate in chalcopyrite-2 is marked by frame. Py, pyrite; Chpy, chalcopyrite; Gal, galena; For, fahlore; Pr + Hzw, aggregate of pyrrhotite and heazlewoodite. Length of scale ruler is 500 μm.

tions of these elements vary; however, they always occur in elevated amounts. Sb and, rarely, As are prevalent among semimetals. The stably elevated Cr and Ni contents in ore are noteworthy. The Te and Bi contents in ore are low, no higher than 3–5 gpt in single samples. Cd is a significant admixture in ore; its content reaches 0.346 wt % in certain samples. Its distribution is directly controlled by the sphalerite content. The Ba concentrations are at level of the first few tens of gpt; the Sr content in most samples is below the detection limit.

The Au and Ag concentrations in certain samples reach 30 and 326 gpt, respectively, although in the majority of analyzed samples, the Au contents vary within 0.12–8.5 gpt. The mean concentrations based on analyses of 48 samples are 3.35 gpt Au and 100.5 gpt Ag (Table 4). As follows from the Au/Ag ratios, ore of the deposit is enriched in silver. This ratio mostly falls in the interval of 0.1–0.01; the average value is about 0.03. A weak positive correlation of Au + Ag sum and total Fe is noteworthy ($r = 0.57$) (Fig. 11).

In addition to quartz–sulfide ore, elevated concentrations of ore-forming components, including Au (up to 1.5 gpt) and Ag (up to 91 gpt), have been established in listvenite. In this case, mineralization is related to thin quartz–sulfide stringers in metasomatic rocks. In the geochemical and mineralogical aspects, ores related to quartz–sulfide veins and stringers in listvenite boudins are identical. This implies that lithologic control of mineralization does not operate.

GEOCHEMISTRY OF SULFUR AND OXYGEN ISOTOPES

The sulfur isotopic compositions of sulfide minerals at the Zun-Ospa deposit fall within the interval of +2.2 to +5.1‰ (Table 6, Fig 12a). The sulfur isotopic compositions of pyrite and sphalerite vary in a narrower range from +3.7 to +4.4‰. The isotopic composition of galena reveals a relatively wider scatter of +2.2 to +4.3‰. The analyzed chalcopyrite monofractions were selected from chalcopyrite-2 aggregate, which is characterized by a somewhat charging sulfur isotopic composition from +4.4 to +5.1‰.

The formation temperature, as well as the sulfur and oxygen isotopic compositions in an equilibrium

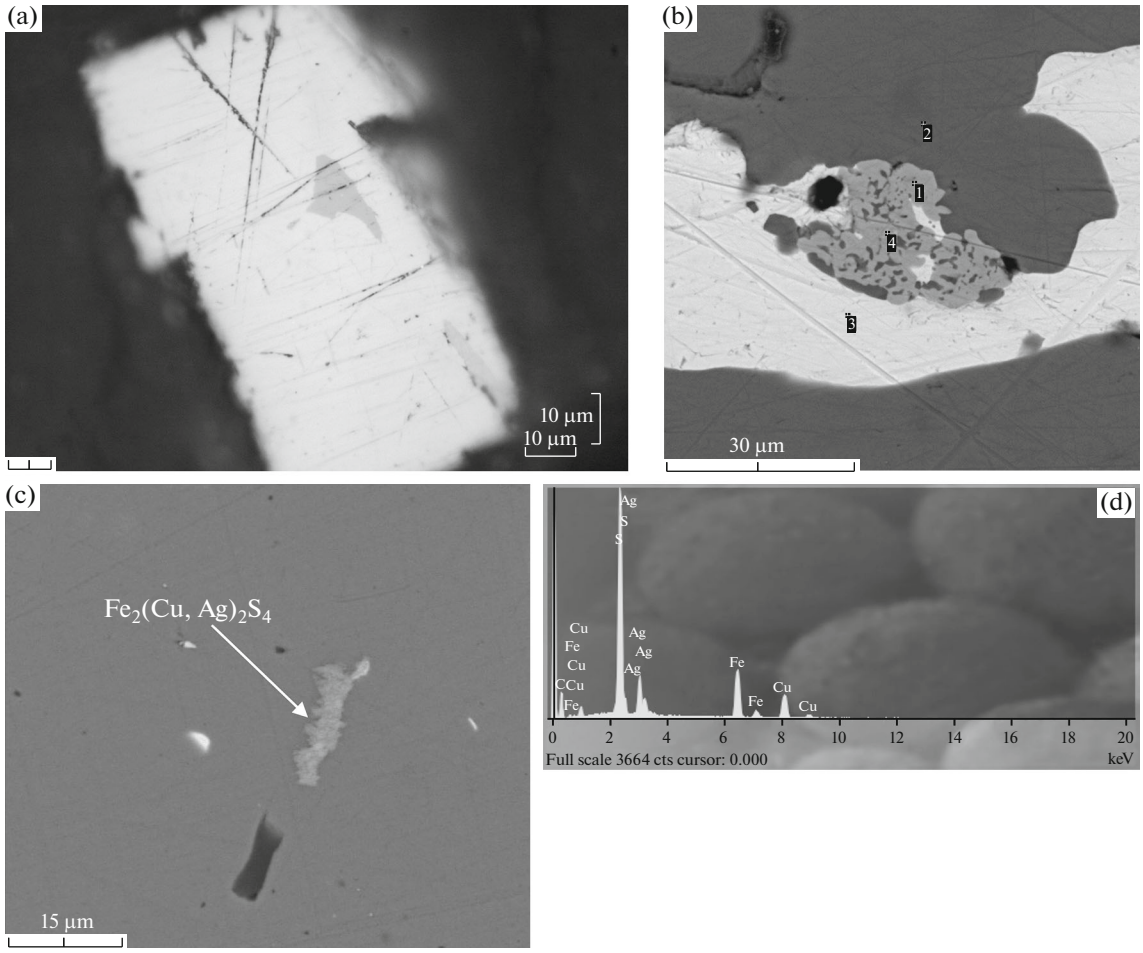

Fig. 7. Minerals of Ag-sulfosalt assemblage: (a) stephanite inclusion in galena, length of scale ruler is 10 μm; (b) skeletal intergrowth of ullmannite (1) and miargyrite (4) in interstices between chalcopyrite (2) and galena (3); (c) morphology of phase $Fe_2(Cu,Ag)_2S_4$, host mineral is pyrite, fine mineral white in color is galena; (d) energy-dispersive spectrum of phase $Fe_2(Cu,Ag)_2S_4$.

fluid, were calculated by an online program (http://www2.ggl.ulaval.ca/cgi-bin/alphadelta/alphadelta.cgi, created by Beaudoin and Therrien, 2004, 2009). The temperature has been calculated using equations by Li and Liu (2006) for the sphalerite–galena couple (sample nos. Zo-221 and Zo-229, see Table 4), the paragenesis of which has been established rather distinctly by mineragraphic study. The temperature value corresponds to 306°C.

According to the classic monograph (G. Faure, 1989), $\delta^{34}S$ of sulfide must decrease in the sphalerite–chalcopyrite–galena series. In order to calculate the sulfur isotopic composition of H_2S in the ore-forming fluid, the isotopic composition of sulfide minerals corresponding to the given succession have been chosen (Table 5). According to equations presented by Ohmoto and Rye (1979) and Li and Liu (2006), calculation was done out in the aforementioned online program. It has been established that the isotopic compositions of H_2S in fluid somewhat differ by distinct mineral parageneses (Fig. 12b). Such minerals as galena, sphalerite, and chalcopyrite-2 are formed from fluids very close to sulfur isotopic composition of H_2S, and at a T about 300°C, isotopic equilibrium is established, where $\delta^{34}S$ of H_2S is about +4.1‰. The sulfur isotopic composition of the pyrite-forming fluid is distinguished by a somewhat lower ^{34}S from +2.2 to 2.8‰.

The oxygen isotopic composition of quartz at the Zun-Ospa deposit falls in a narrow interval from +12.3 to +12.6‰ (Table 5). According to Zhang et al. (1989), the $\delta^{18}O$ for water of the ore-forming fluid calculated for 300°C falls in the interval from +4.9 to +5.2‰.

FLUID INCLUSION STUDY

In quartz and calcite from ore of the Zun-Ospa deposit, rare primary fluid inclusions (FI) have been identified and studied. Searching for them is a difficult task. The studied inclusions, as a rule, are two-phase (aqueous solution > gas phase) and related to of

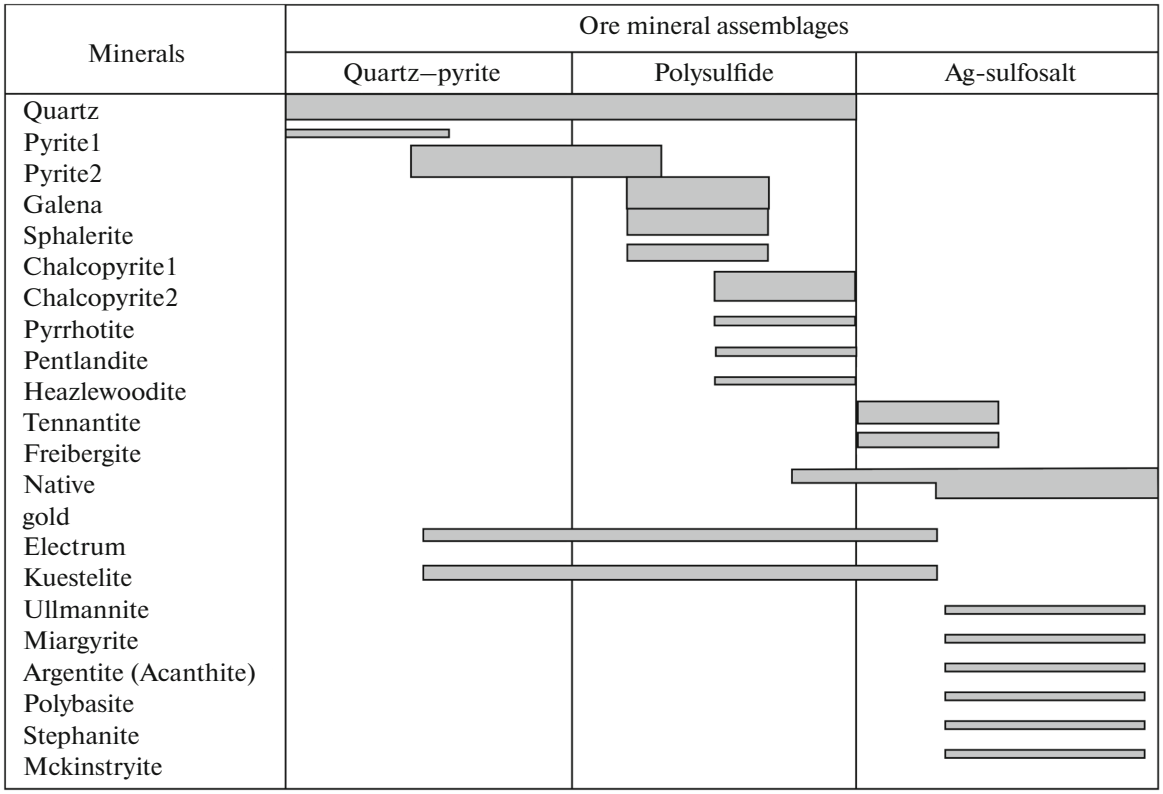

Fig. 8. Succession of mineral formation in ore.

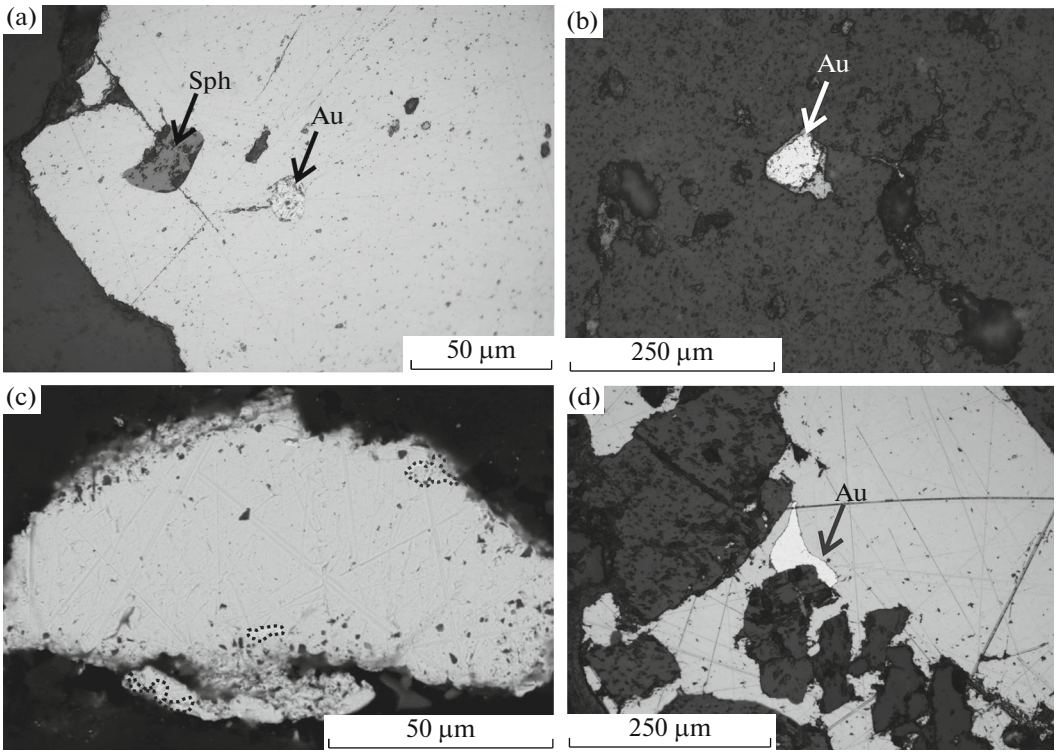

Fig. 9. Morphology of native gold: (a) inclusion of electrum (Au) and sphalerite (Sph) in pyrite-1; (b) grain of native gold in quartz; (c) grain of electrum with stringerlike segregations of native gold (BSE image); (d) grain of kuestelite (Au) in galena.

Table 4. Chemical compositions of gold minerals

No.	Sample	Au	Ag	Total	Probability, ‰
Oxidized ore (quartz with supergene minerals)					
1	30_206-1	85.35	14.55	99.90	854
2	30_206-2	85.27	15.07	100.35	850
3	30_206-3	85.10	15.18	100.28	849
4	30_206-4	84.28	15.16	99.45	848
5	30_206-5	84.90	15.54	100.45	845
6	30_206-6	83.96	15.65	99.61	843
7	30_206-7	77.90	22.56	100.47	775
8	30_206-8	76.09	23.69	99.78	763
9	30_206-9	76.67	23.88	100.55	763
10	30_206-10	73.42	26.09	99.51	738
11	30_206-11	72.38	28.26	100.64	719
12	30_206-12	69.62	30.19	99.81	698
13	30_206-13	65.50	34.30	99.80	656
14	30_206-14	63.89	36.95	100.85	634
15	30_206-15	62.38	37.66	100.04	624
16	30_206-16	61.90	38.93	100.82	614
17	30_206-17	58.53	41.57	100.09	585
18	30_206-18	54.01	46.94	100.95	535
19	30_206-19	52.59	46.90	99.51	529
20	30_206-20	53.10	47.62	100.72	527
21	30_206-21	51.62	48.37	99.99	516
22	30_206-22	50.35	48.63	98.98	509
23	30_206-23	50.66	49.19	99.86	507
24	30_206-24	50.82	49.95	100.78	504
25	30_206-25	49.94	49.57	99.51	502
26	30_206-26	49.39	50.14	99.54	496
27	30_206-27	49.20	50.16	99.36	495
28	30_206-28	49.33	51.09	100.42	491
29	30_206-29	49.01	51.26	100.28	489
30	30_206-30	47.94	51.44	99.38	482
31	30_206-31	47.75	52.36	100.11	477
32	30_206-32	47.09	52.12	99.23	475
33	30_206-33	47.73	52.88	100.60	474
34	30_206-34	47.39	52.90	100.29	473
35	30_206-35	47.20	52.94	100.13	471
36	30_206-36	47.22	53.00	100.23	471
37	30_206-37	47.04	52.80	99.83	471
38	30_206-38	46.81	53.26	100.08	468
39	30_206-39	47.09	53.67	100.77	467
40	30_206-40	45.89	54.41	100.30	458
41	30_206-41	45.65	54.51	100.16	456
42	30_206-42	45.23	54.95	100.18	451
43	30_206-43	44.67	54.35	99.03	451

Table 4. (Contd.)

No.	Sample	Au	Ag	Total	Probability, ‰
44	30_206-44	44.56	55.88	100.44	444
Mean value of probability					**585**
Standard deviation					**142**
Asymmetry coefficient					**0.88**
Low-sulfide quartz veins					
45	30_213	77.43	22.94	100.37	771
46	30_203-1	85.33	14.86	100.19	852
47	30_203-2	57.96	42.42	100.38	577
48	30_203-3	52.24	47.88	100.12	522
49	30_202	49.82	50.46	100.28	497
50	30_219-1	45.37	54.50	99.87	454
51	30_219-2	45.29	54.67	99.96	453
52	30_202-1	45.56	55.19	100.73	452
53	30_202-2	44.48	55.75	100.23	444
Mean value of probability					**531**
Standard deviation					**151**
Asymmetry coefficient					**1.38**
Quartz–polysulfide ore					
54	zo210-1	44.38	55.72	100.10	443
55	zo210-2	43.94	56.60	100.53	437
56	zo210-3	43.26	56.76	100.01	432
57	zo210-4	43.25	56.81	100.06	432
58	zo210-5	41.79	57.18	98.97	422
59	zo210-6	40.12	59.07	99.19	404
60	zo210-7	39.82	60.27	100.09	398
61	zo210-8	38.97	60.36	99.35	392
62	zo210-9	39.17	61.13	100.30	391
63	zo210-10	37.62	62.76	100.38	375
64	zo210-11	37.17	62.92	100.09	371
65	zo210-12	36.81	63.14	99.94	368
66	zo210-13	35.82	64.45	100.28	357
67	zo210-14	35.67	64.83	100.49	355
68	zo210-15	31.59	68.82	100.41	315
69	zo210-16	30.72	69.85	100.57	305
70	zo210-17	30.25	70.24	100.49	301
71	zo210-18	14.35	84.85	99.19	145
72	zo210-19	13.93	86.67	100.60	138
73	Zo-226-1	24.98	75.02	100.00	250
74	Zo-226-2	24.92	75.08	100.00	249
75	Zo-226-3	21.14	78.86	100.00	211
76	Zo-226-4	19.39	80.61	100.00	194
Mean value of probability					**357**
Standard deviation					**94**
Asymmetry coefficient					**–0.84**

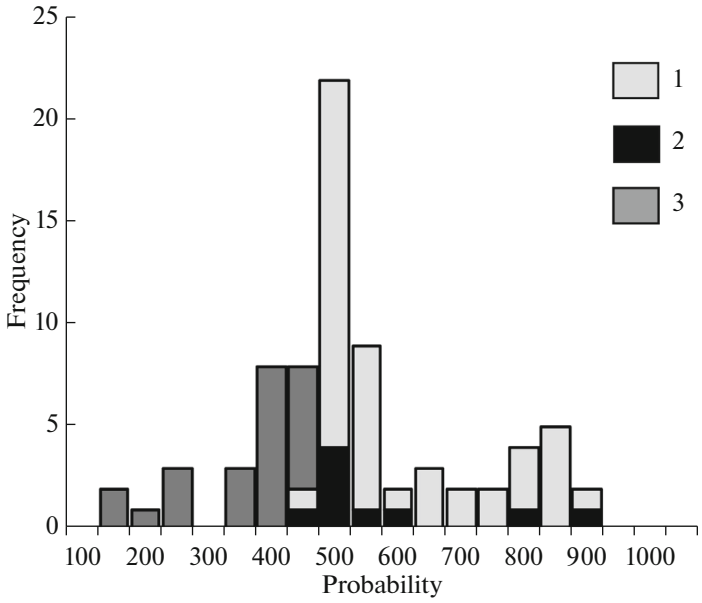

Fig. 10. Histogram of distribution of native gold fineness: 1, gold from oxidized ore; 2, gold from low-sulfide quartz veins; 3, gold from quartz–polysulfide veins.

homogeneous trapping inclusions. In a majority of cases, the primary FIs are identified as single isometric and rare elongated inclusions. They are minor in dimensions, which vary from a few μm to, very rarely, 6–8 μm (Fig. 13). More than 40 primary inclusions have been studied in various samples, but for some of them, we failed to obtain necessary measurements due to bad visibility and/or minor dimensions, or else we succeeded in recording only some of the parameters, e.g., the homogenization temperature (Table 7).

In addition, trains of numerous minor (a few μm) secondary inclusions likely recording sealed fractures or heterogeneities are observed in quartz grains. Unrepresentative inclusions intersected by such trains or fragmented FIs clustered in flattened trains (sealed microfractures) are referred to the group of secondary inclusions, which were not studied by us.

Based on the conducted thermometric experiments, the general interval of the homogenization temperature (T_{hom}) for inclusions was established as 445–250°C in quartz. For several inclusions in calcite, the temperature varies from 355 to 240°C (Table 6). In general, most determinations fall in the interval of 200–380°C with two peaks in intervals of 240–280°C and 320–380°C (Fig. 14). Some of the inclusions are decrepitated at a temperature from 230 to 385°C.

Cryometric studies have shown that temperature of ice melting ($T_{melt.ice}$) in inclusions from quartz and carbonates vary from –3.2 to –10.2°C. Consequently, the general salinity of solutions changes from 5.3 to 14.2 wt % NaCl equiv. The eutectic temperature (T_{eut}) varies from –33.2 to –38°C (Table 6) and assumes that trapped solutions are close to the systems $MgCl_2$–$NaCl$–H_2O, $MgCl_2$–KCl–H_2O, $NaCl$–$FeCl_2$–H_2O or $FeCl_3$–H_2O (Kirgintsev et al., 1972; Borisenko, 1977). In the temperature interval of –21.2...–23.5°C, an abrupt intensification of ice thawing is recorded, which is evidence for the presence of NaCl and/or KCl in solution (Borisenko, 1977).

DISCUSSION

The Zun-Ospa deposit is characterized by distinctly expressed structural control of mineralization. All ore zones and bodies are localized in mélange consisting of blocks of listvenite, propylitized intermediate and basic rocks, altered granites, and limestones

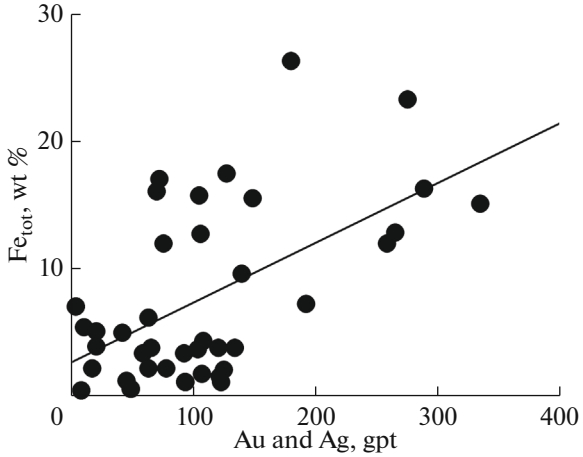

Fig. 11. Correlation of Fe_{tot} (wt %) and total Au and Ag (gpt) in ore from the deposit.

Table 5. Contents of admixture elements in ore of Zun-Ospa deposit, ppm

No.	Sample	Ba	Rb	Sr	Zr	Y	Cr	Ni	Co	V	Cu	Pb	Zn	Cd	Sn	Mo	Ag	Au	As	Sb	Te	Fe,%
1.	zo-225	8					52	136	111	11	52000	70000	13000	186		6	264.0	0.50		127	3	12.9
2.	zo-226	10					240	117	100		68000	35000	5300	120			252.0	6.00		81		12.1
3.	zo-227	26	16		12	15	333	17	14	4	850	3800	42000	990		3	16.0	1.50		20		2.3
4.	zo-12	15			13		355	48	4	4	57	28000	2300	52	3		45.0	0.36		12		1.3
5.	zo-17	48			25		228	21	8	4	62	12000	260	9			7.1			57		3.2
6.	zo-20	23		38	20	14	318	180	7	7	16	10000	1400	10			46.0			12		1.4
7.	zo-201	29	7		9		395	17	1	5	68	6200	31	5			48.0	1.20		13		0.7
8.	zo-202	46			7		376	15	1		43	16000	54				86.0	7.30		76	2	1.2
9.	zo-203	87					376	15	1	4	43	19000	510				162.0	30.00		81	7	7.3
10.	zo-205				12		41	27	4	6	600	98000	13000	22			273.0	2.30		180	3	23.3
11.	zo-206	12		840			113	70	30	23	800	32000	4000				282.0	6.00		200		16.4
12.	zo-209	2			20		385	110	40	12	690	13000	4600	175			326.0	8.50	250	37		15.2
13.	zo-210	25			11		172	170	58		2400	3800	6000	150			176.0	4.00	250	23		26.3
14.	zo-211						32	39	157	5	1700	21000	20000	2570			108.0	0.30	1000	465		4.4
15.	zo-212	60					85	264	49	8	36000	85000	63000	430			58.0	1.00		50	5	3.5
16.	zo-213	54	8		6	17	295	38	5	5	160	2500	310	10	3		75.0	3.00		50		2.3
17.	zo-214	11					335	72	52		12000	124000	19000	260			62.0	1.50	500	255		6.2
18.	zo-215	19					116	29	38	6	18400	72000	290000	3460			92.0	0.90		180		3.5
19.	zo-216	11	3		2	3	278	16	1	4	39	240	72	1		1	9.0	0.01		3		0.6
20.	zo-218	7	29		7		215	20	6	5	2500	19000	13000	265			119.0	2.50		48		1.6
21.	zo-219	22			8		383	132	29	14	900	7300	1260	45			61.0	2.00		110		2.3
22.	zo-221	20					89	48	63	20	230	10000	30 000	2940			117.0	3.00		420		3.9
23.	zo-222	25	37				173	36	13		1600	13000	16000	256			20.0	1.50		44		4.0
24.	zo-223	19	32		34		234	39	10	5	76000	12000	3600	82		5	150.0			85		10.0
25.	zo-228						587	395	36	15	2100	34000	24000	740			139.0	1.00		70		9.7

Table 5. (Contd.)

No.	Sample	Ba	Rb	Sr	Zr	Y	Cr	Ni	Co	V	Cu	Pb	Zn	Cd	Sn	Mo	Ag	Au	As	Sb	Te	Fe,%
26.	zo-234	25					148	48	46	5	500	21000	7100	230		5	144.0	4.55		38		15.6
27.	zo-236	320	21	8	24	22	143	21	17	26	354	2500	2650	210		36	20.0	1.50		13		5.2
28.	zo-237	56					161	50	56	10	310	57000	7300	230		3	125.0	2.00		71	2	17.5
29.	zo-239	167					92	34	51	19	445	26000	12000	700		52	69.0	3.00		39		17.1
30.	zo-24	117	8	2	15		230	26	3	15	26	147	110				2.0					1.8
31.	zo-241	150	28		4		131	27	47	19	340	11000	8300	550		43	67.0	3.00		28		16.1
32.	zo-242	230					116	103	109	19	470	24000	71000	1000			104.0	1.00		31		15.8
33.	zo-246	350			18		130	11	4	18	490	5000	330	19	3	61	123.0	0.15		14		1.2
34.	zo-247	410			20		102	13	6	16	280	8800	14000	320		5	125.0	0.45		28		2.2
35.	zo-249	41	8		15		224	49	42	8	290	4900	4060	169		61	76.0	0.07	285	20		12.0
36.	zo-25	96	8		11	18	513	31	1	8		2000	250	3			57.0			13		1.7
37.	zo-250	86	12		14	23	173	26	16	8		3300	1450	64		15	64.0	1.60		10		3.9
38.	zo-251	7	9		6	15	280	42	22	9		1700	620	11			42.0	0.70		6		5.1
39.	zo-27	4		3	6	1	330	169	8	8		67	2800	28			1.0			4		1.2
40.	zo-29	16			18	13	168	32	18	13		5300	5800	95		4	11.0	0.12		36		5.5
41.	zo-30	20			15	10	276	47	39	18		4700	900	20	1	2	133.0			22		3.1
42.	zo-31	15			49		175	48	20	24		11200	43200	540	2	3	137.0			55		5.1
43.	zo-32	15			13		261	43	7	8		8000	1100				96.0	8.00		32		3.8
44.	zo-33	15			10		743	31	4	13		5600	700				106.0	1.60		34		1.8
45.	zo-34	19			20		319	106	45	11		45000	81200	860			128.0	6.00		145		3.9
46.	zo-35	8			25		238	49				17000	5100	113	2		99.0	7.50		52	9	12.8
47.	zo-36	28			9		347	114		5		4072	6941	270		1		4.80		14		7.6
48.	zo-38						1950	2600		12		25	53				0.3	3.60	5	2		7.1
	D.L.	**3-6**	**3-5**	**3-5**	**3-5**	**3-5**	**10**	**2**		**2**		**10**	**15**	**1**	**1-3**	**1-2**	**0.1**	**0.01**	**5**	**2-3**	**3-5**	**0.5**

Blank cell, not detected; D.L., detection limit, ppm.

Table 6. Isotopic composition of sulfide sulfur in ore and of oxygen in quartz at Zun-Ospa deposit

Sample	$\delta^{34}S$, ‰	$\delta^{18}O$, ‰	$\delta^{34}S$ and $\delta^{18}O$ equilibrium fluid* (H_2S and H_2O, respectively) at $T = 300°C$		Mineral
			$\delta^{34}S$	$\delta^{18}O$	
Zo-211	+4.3		+6.2		Galena
Zo-229**	+2.2		+4.1		Galena
Zo-223	+3.1				Galena + sphalerite
Zo-247	+3.7				Galena + sphalerite
Zo-209	+4.4		+3.2		Pyrite
Zo-210**	+3.7		+2.5		Pyrite
Zo-237	+3.8		+2.6		Pyrite
Zo-214	+3.7		+3.4		Sphalerite
Zo-221**	+4.4		+4.1		Sphalerite
Zo-225	+5.1		+4.9		Chalcopyrite
Zo-35**	+4.4		+4.2		Chalcopyrite
Zo-12		+12.3		+4.9	Quartz
Zo-202		+12.5		+5.1	Quartz
Zo-213		+12.6		+5.2	Quartz
Zo-219		+12.4		+5.0	Quartz

Analyses of sulfur isotopes were carried out at Far East Geological Institute, Far East Branch, Russian Academy of Sciences (analyst T.A. Velivetskaya); analyses of oxygen isotopes were performed at Geological Institute, Siberian Branch, Russian Academy of Sciences (analyst V.F. Posokhov).

* Calculated data after (Li and Liu, 2006; Zhang et al. 1989).

** $\delta^{34}S$ values used in Fig. 12b.

cemented by mylonites after granites and mafic–ultramafic rocks. The strike of orebodies is nearly concordant with that of tectonites, and this indicates their almost synchronous formation. Lithologic control of mineralization is absent, so that blocks differing in composition contain the same quartz–polysulfide mineralization. Granitic rocks within the ore field have also been subjected to tectonic comminution. Their age corresponds to late Neoproterozoic (788 Ma), whereas the age of mineralization is Late Paleozoic (352 Ma). Thus, the formation of ore zones and bodies is not related to magmatic activity; the mélange was caused by tectonic rock deformations. The boudinlike morphology of certain quartz–sulfide bodies allows us to

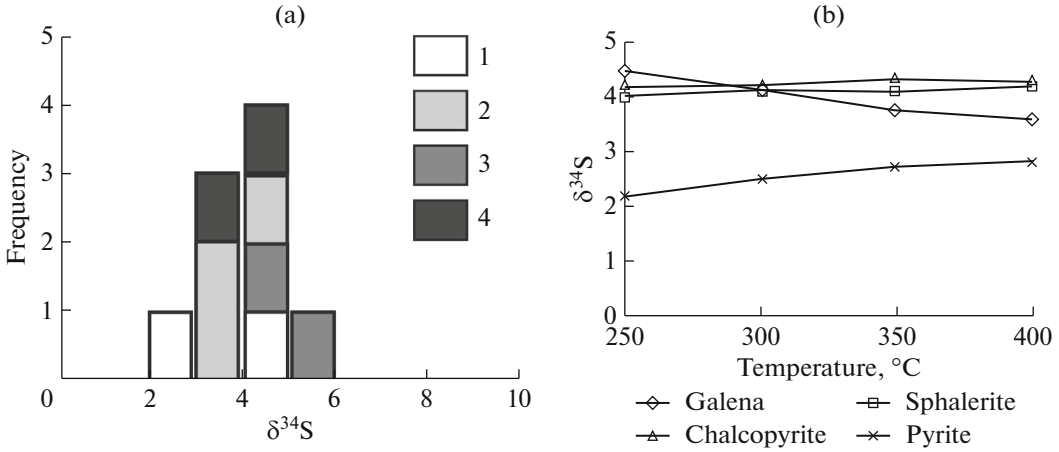

Fig. 12. Features of sulfide sulfur isotopic composition: (a) histogram of sulfur isotopic composition in sulfides: (1) galena, (2) pyrite, (3) chalcopyrite, (4) sphalerite; (b) distribution of calculated sulfur isotopic composition in H_2S of ore-forming fluid, which produces various minerals depending on temperature.

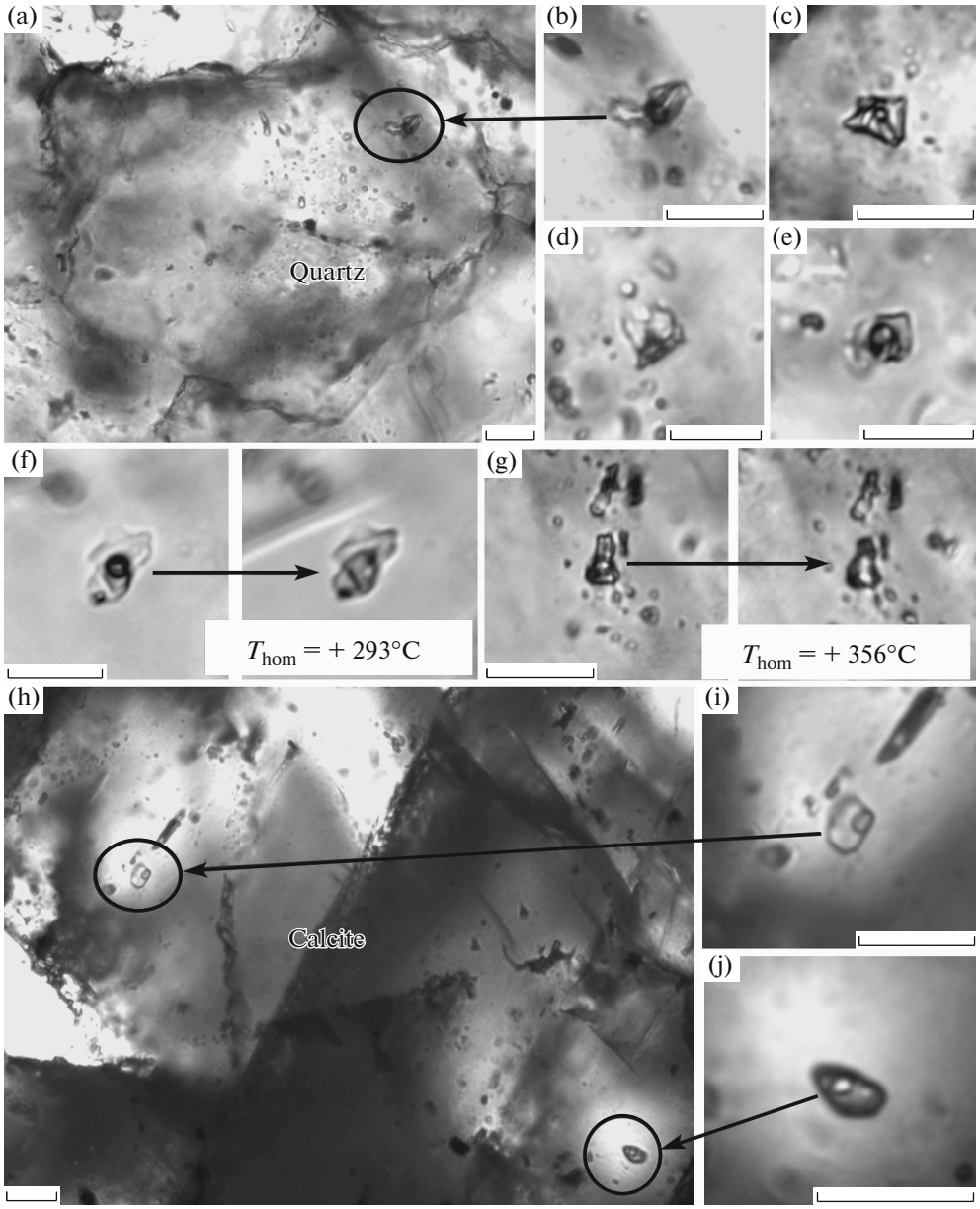

Fig. 13. Photomicrographs of primary fluid inclusions in quartz (a–g) and calcite (h–j): a, quartz grain with primary inclusion in marginal part; a, b, d, e, typical primary inclusions in quartz; f, g, homogenized inclusions; h, calcite grain with primary fluid inclusions; i, j, inclusions in calcite. Length of scale ruler is 10 μm. T_{hom} is homogenization temperature.

suggest the occurrence of sulfide mineralization at the pretectonic stage of the ore field's development. Indeed, gold-bearing stratiform sulfide ores are known in the studied region (Olgino and Ilchir ore occurrences, early ore at the Zun-Kholba deposit, etc.). They are composed of pyrrhotite aggregates with an admixture of chalcopyrite and, to a lesser degree, arsenopyrite, sphalerite, galena; they are products of hydrothermal–sedimentary ore formation in a back-arc basin spreading zone (Mironov et al., 1999).

The study of the ore mineralogy at the deposit allows us to recognize three stages of ore formation: (i) early quartz pyrite, (ii) quartz polysulfide, and (iii) late Ag-sulfosalt. The earliest Au-bearing quartz–pyrite assemblage comprises early quartz and pyrite-1, which does not contain sulfide microinclusions (galena, sphalerite, etc.). The intermediate quartz–polysulfide assemblage is characterized by maximum gold and silver concentrations and is thus the most productive. In addition, the identified native gold grains are related to minerals of a polysulfide assemblage, primarily, galena, where the proportions of these minerals allow us to suggest their joint formation. The late Ag-sulfosalt assemblage is characterized by a minor distribution of minerals and the presence of relatively high-fineness gold. The occurrence of sul-

Table 7. Results of thermobarogeochemical fluid inclusion studies

No.	Sample	$T_{eut.}$	$T_{melt.ice}$	$T_{hom.}$	$T_{decr.}$	Salinity, NaCl equiv.	Suggested salt systems
1.	Zo-33-1	–36			281		$MgCl_2$–NaCl–H_2O,
2.	Zo-30-1	–34.5 and –22			270		$MgCl_2$–KCl–H_2O,
3.	Zo-29-1	–33.2 and –21.3	–4.5	250	253	7.2	NaCl–$FeCl_2$–H_2O,
4.	Zo-30-1		–5.6...–4.8	355		8.1	$FeCl_2$–H_2O,
5.	Zo-29-1	–35.5 and –23.7			293		$FeCl_3$–H_2O,
6.	Zo-20-1	–21	–2.8...–3.2	293		5.0	NaCl–H_2O,
7.	Zo-17	–22	–6...–5	370		8.6	KCl–H_2O
8.	Zo-17	–23..–22	–5	396		7.9	
9.	Zo-17	–36 and –18	–6.3	390		9.6	
10.	Zo-17	–22.3	–5.1	360		8.0	
11.	Zo-17	–23.6	–8	390		11.7	
12.	Zo-17	–21	–9...–8	370		12.3	
13.	Zo-17	–37...–36	–6.5...–6		363	9.5	
14.	Zo-17	–21		375			
15.	Zo-17	–21	–6.5	170		9.9	
16.	Zo-12	–21.8	–6.9	330		10.4	
17.	Zo-12	–35	–7	356		10.5	
18.	Zo-12	–32 and – 25	–7...–5.5	290		9.6	
19.	Zo-20	–21.5...–22.5	–8...–7	350		11.1	
20.	Zo-29	–36...–35 and –3.7			230		
21.	30-29	–26			385		
22.	30-17	–37		275			
23.	30-17			375			
24.	30-17	–27	–9.6	383		13.5	
25.	30-17	–36	–10.2	280	532	14.2	
26.	30-30	–38	–8.5	295	317	12.3	
27.	30-218	–36.4		445			
28.	30-218	–37		350	370		
29.	30-218	–37		340			
30.	30-218	–38	–9.5	360		13.4	
31.	30-218		–8.1	365		11.8	
32.	30-218	–27	–8.7	302		12.5	
33.	Zo-20			355			
34.	Zo-20	–36.7 and –25			144		
35.	Zo-20	–35.5	–3.3	240		5.4	
36.	Zo-20	–21	–3.2	293		5.3	

1–32, fluid inclusions in quartz; 33–36, in carbonates. Temperature, °C: $T_{eut.}$, eutectic; $T_{melt.\ ice}$, melting of ice; $T_{hom.}$, homogenization; $T_{decr.}$, decrepitation. Blank cell, parameter not detected.

fosalts in ore at gold deposits of various types, as a rule, follows crystallization of the galena–sphalerite–chalcopyrite assemblage (Gamyanin, 2001), as is observed in ore of the Zun-Ospa deposit.

Native gold in this deposit is characterized in general by a low fineness. Kuestelite and electrum are the predominant Au–Ag minerals in quartz–polysulfide ore. Fineness increased at the late stage of ore formation, caused by deposition of an Ag-sulfosalt assemblage in which silver is related sulfosalts and relatively high-fineness gold is deposited in a quartz matrix. Similar compositions and statistical parameters of the gold fineness distribution in quartz veins and oxidized ore show stability of late gold with respect to supergene

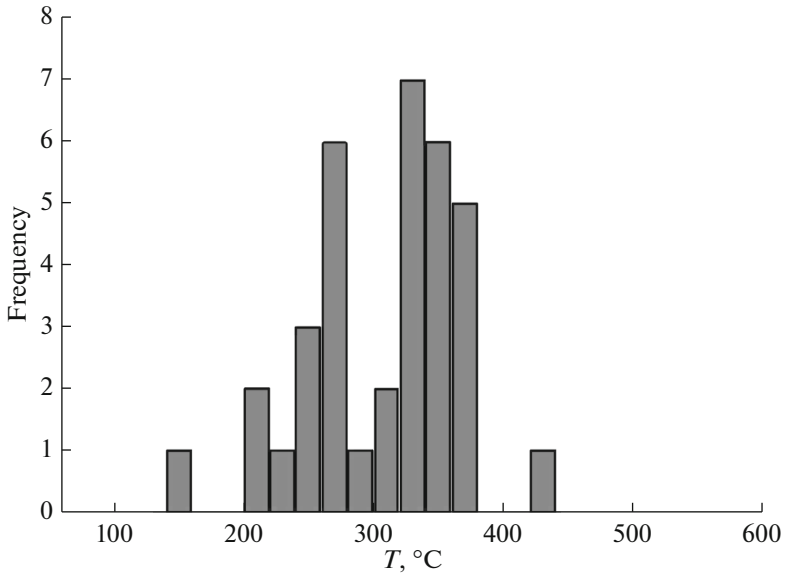

Fig. 14. Histogram of distribution of fluid inclusion homogenization temperature.

processes, whereas early gold in the polysulfide assemblage is removed during sulfide oxidation and redeposited in the weathering mantle. A characteristic morphological feature of gold minerals is the absence of xenomorphic or fractured forms, and this indicates either a relatively deep-seated formation of mineralization or free growth of native gold (Petrovskaya, 1973).

Four elements (Fe, Pb, Zn, Cu) in various proportions dominate in the chemical composition of ore. Lower Te and Bi contents have been established by means of analytical methods, as well as by ore mineralogy. In particular, Bi- and Te-containing mineral phases have not been revealed. This, along with low Mo, Sr, and Ba concentrations, rule out the effect of granitic magmatism on ore formation. In addition, Ni and Cr occur in elevated amounts as evidence for a gain in ultramafic materials. The occurrence of these elements may be linked only to redistribution of components due to tectonic transformation of mafic and ultramafic rocks of the ophiolitic association, because other possible sources of these elements are not known in the ore field.

The temperature interval of 380–200°C established by FI studies and isotopic geothermometers corresponds to the minimum temperatures of vein quartz formation. The peaks marked in the histogram of the homogenization temperature distribution correspond to various quartz deposition stages (Fig. 13). The high-temperature peak (380–320°C) fits the minimum temperature of early coarse-grained quartz deposition, whereas deposition of the second fine-grained generation falls in a temperature interval higher than 280–240°C. The total salinity of ore-forming solutions is not high and varies within 5.2–14.2 wt % NaCl equiv. Mg and Fe chlorides with admixtures of Na and K predominate in the salt composition of ore-forming solutions, whereas carbon dioxide concentrations are lower. Close eutectic temperatures (–34 to –37°C) and, consequently, Mg–Fe-chloride compositions of hydrothermal solutions have been established for FIs in quartz from metamorphosed submarine hydrothermal–sedimentary sulfide (pyrrhotite) ore in the upper volcanic–sedimentary sheet of the ophiolitic complex in the Eastern Sayan (Mironov et al., 1999).

The early quartz generation contains ore gold–pyrite-1 assemblage, whose temperature of deposition is 380–320°C. The gold–polysulfide assemblage appears later, when temperature of galena–sphalerite assemblage is estimated at 306°C. Because pyrite-2 is formed obviously earlier than galena–sphalerite assemblage but later than pyrite-1, the temperature of its deposition should be intermediate and according to obtained thermometric data corresponds to 320–300°C. Taking into consideration that the FI homogenization temperature reflects the minimum values of the parameters characterizing ore quartz deposition, the temperature of late quartz deposition is comparable with the formation temperature of the main productive gold–polysulfide assemblage. This allows us to regard the interval of 320–240°C, as the most probable formation temperature of the latter. The Ag-sulfosalt assemblage with relatively high-fineness gold formed at the late low-temperature stage. The formation temperature interval of this assemblage is determined by the upper boundary of stephanite stability, i.e., 197°C (Keighin and Honey, 1969). Available single determinations of homogenization and decrepitation temperatures near 170–144°C likely reflects the

minimum conditions of Ag-sulfosalt assemblage deposition.

The sulfur isotopic compositions in sulfide are close to sulfur from primary sulfide ore in the upper sheet of the ophiolitic complex, interpreted as ancient black smoker deposits (Mironov et al., 1999; Mironov and Zhmodik, 1999). Present-day submarine sulfide deposits have a close isotopic composition (*Gidrotermal'nyi rudogenez* ..., 2006; Seal, 2006). At the same time, calculation of the sulfur isotopic composition in H_2S of an equilibrium fluid allows us to reveal certain distinctions in early and late ore assemblages. Thus, the fluid that formed the early quartz–pyrite assemblage is characterized by a relatively light-weight isotopic composition of sulfur ($\delta^{34}S$ is ~2‰), whereas sulfur from polysulfide is relatively enriched in ^{34}S ($\delta^{34}S$ is about 4‰). Such distinctions can be explained by the appearance of heavy sulfur isotopes.

The oxygen isotopic composition in vein quartz recalculated to the composition of the equilibrium fluid yields about 5‰. These values are close to the composition of juvenile water (Hoefs, 2009), but are somewhat depleted in ^{18}O, likely due to interaction with meteoric waters.

However, close isotopic composition values can be acquired by solutions of mixed meteoric–metamorphic genesis, and in the given case, this is more likely, taking into account that quartz veins formed under conditions of intense tectonic deformations, in the course of which primary minerals from mantle-derived rocks (ophiolites) are comminuted and metamorphosed with the formation of a duplex mélange structure permeable to meteoric waters.

The measured isotopic ratios are a consequence of transformation of rocks differing in composition and genesis within the tectonic mélange zone, varying from fragments of sulfide structures and mantle-derived ultramafic rocks to granitic and metamorphic sedimentary rocks. Intense tectonic deformations of rocks yielded a gain in metamorphic–hydrothermal solutions, which leached and redeposited ore-forming components. The nonmagmatic nature of the ore-forming solutions is also supported by the fact that igneous rocks close in age to the ore are not exposed in the ore field. It should be mentioned that the largest gold–sulfide–quartz deposits in the region (Zun-Kholba, Pioneersky, Vodorazdelny) are also characterized by an identical sulfur isotopic composition (Mironov and Zhmodik, 1999), corresponding to that of black smoker ores. Here, it is noteworthy that the phase composition of submarine sulfide bodies with such predominant minerals as pyrite, pyrrhotite, sphalerite, chalcopyrite, and galena correspond to the ore composition at the Zun-Ospa deposit.

As a result, such indications as close ore mineralogy, similar Mg–Fe-chloride salt compositions of solutions, and identical isotopic parameters allow us to consider metalliferous sediments of ancient black smokers as one of the leading sources of matter for the Zun-Ospa gold–polysulfide deposits and their counterparts (Zun-Kholba, Vodorazdelny, and etc.) in the region localized within outcrops of rocks pertaining to the ophiolitic association. Fragments of primary hydrothermal–sedimentary sulfide ore have been recorded at almost all of these deposits.

The formation of ophiolites making up the Ospino–Kitoi massif is linked to the development of the Dunzhugur island arc; the time of its existence is dated at 1020–800 Ma (Kuz'michev and Larionov, 2013, Khain et al., 2002). According to known paleogeodynamic reconstructions, the obduction of ophiolites happened at the Early Baikal stage of evolution about ~800 Ma ago due to collision of the Gargan continental block with the Dunzhugur island arc (Fedotova and Khain, 2002). Intrusion of granitic rocks belonging to the Sumsunur Complex has been dated at a close but relatively late period of time (~790 Ma). The observed relationships of tectonites with adjacent rock complexes, as well as the results of geochronologic studies, provide evidence that the formation of tectonic mélange obviously happened after the obduction of ophiolites and intrusion of granitic bodies. The completing stage of evolution is dated at the Late Paleozoic (352 Ma). This age reflects a time of post-collision shear deformations in the Central Asian Foldbelt, caused by collision of the Kazakhstan–Baikal and Siberian continents (Buslov, 2011). The structural scheme of the Zun-Ospa deposit indicates the formation of mineralization in the strike-slip duplex zone, which controls the localization of basic mineralization. The formation of such structures was caused by the development of near-parallel strike-slip faults, between which oblique faults operate (Znamensky and Znamenskaya, 2011). The Au-bearing quartz–sulfide veins were deposited and quartz–sulfide mineralized zones were formed by the release of pressure. A relationship between gold mineralization and strike-slip structures is also distinctly shown at other gold deposits of the region, in particular, at the Kholba ore field (Zhmodik et al., 2006).

On the basis of geological, mineralogical, and geochemical indications, the deposit is related to the gold–polysulfide mineral type or to the type of orogenic mesothermal deposits, the formation of which is also related to accretionary–collision settings (Groves et al., 1998; Ridley and Diamond, 2000). Such deposits frequently do not reveal a visible link with magmatic activity (Goldfarb et al., 2005). It has been suggested that the formation of these objects was caused by the appearance of metamorphic hydrothermal ore-forming fluids due to dehydration of rocks in the course of metamorphism pertaining to greenschist and epidote-amphibolite facies (Beaudoin and Pitre, 2012; Goldfarb et al., 2005; Phillips and Powell, 2010; Ridley and Diamond, 2000).

A similar metamorphic–hydrothermal genetic nature of mineralization was most likely during the formation of Zun-Ospa deposit. In this case, the release of metamorphic fluid was caused by dynamometamorphism, giving rise to the formation of the host mélange. Sources of ore-forming components were rocks subjected to deformations, among which fragments of an ophiolitic nappe are predominant, including relics of submarine sulfide bodies; granitic and terrigenous–carbonate rocks occur as well. It is known that hydrothermal rocks of back-arc spreading zones are characterized by elevated concentrations of such chemical elements as Au, Ag, Fe, Cu, Zn, and especially Pb (*Gidrotermal'nyi rudogenez ...*, 2006), i.e., elements typomorphic of ore of the Zun-Ospa deposit. In addition, rocks of the ophiolitic complex of the Eastern Sayan themselves are also characterized by elevated gold contents (Grebenshchikova and Shmotov, 1997; Mironov and Zhmodik, 1999; Zhmodik et al., 2008; Mironov et al., 2002). Other orogenic deposits in the region, which are characterized by close compositions of mineralization, geological position of orebodies, and isotopic geochemical features of ore, have a similar genesis.

CONCLUSIONS

(1) The Zun-Ospa gold deposit is related to a tectonic mélange zone that formed mostly after rocks of ophiolitic associations with the addition of granitic and terrigenous–carbonate rocks. Among the rocks making up the mélange, blocks of ophiolites with fragments of primary hydrothermal–sedimentary sulfide ore and granitic rocks of the Sumsunur Complex with a small admixture of terrigenous–carbonate rocks are predominant. Structural control of mineralization is clearly expressed at the deposit without visible link to magmatic activity.

(2) Three mineral assemblages are distinguished in ores: gold–quartz–pyrite, gold–quartz–polysulfide, and Ag-sulfosalt. They formed against a background of an overall drop in temperature within an interval of 380–170°C from slightly saline solutions (5.2–14.2 wt % NaCl equiv.). Mg and Fe chlorides with additional Na and K are salt components.

(3) Gold minerals are represented by kuestelite, electrum, and low-fineness native gold. The gold fineness increases at the late stage of ore formation owing to the formation of the silver sulfosalt assemblage.

(4) The sulfur isotopic composition is +2.2 to 5.1‰ and is close to that of orogenic gold deposits. The oxygen isotopic composition in quartz is 12.3–12.6‰. Calculation of the sulfur isotopic composition in H_2S and oxygen in water of the ore-forming fluid provides evidence for various sources of matter. It is suggested that sulfur is supplied from primary sulfide ore occurring in ophiolites and from a mixed source composed of rock subjected to dynamometamorphism during tectonic deformations. The ore-forming fluids contain both metamorphic and meteoric waters.

(5) Formation of the deposit took place as a result of redistribution of components in the evolution of a metamorphic–hydrothermal ore-forming system controlled by dynamometamorphism of rocks in the mélange zone related to the strike-slip duplex structure. The appearance of this structure in the Late Paleozoic was caused by postcollision shear deformations within the entire Central Asian Foldbelt.

(6) The mineralogical and geochemical characteristics of the Zun-Ospa gold deposit and its geological position allow us to refer it to the gold–polysulfide mineralization with a metamorphic–hydrothermal genesis.

ACKNOWLEDGMENTS

The research was supported by the Russian Foundation for Basic Research (project no. 18-05-00489).

REFERENCES

Airiyants, E.V., Zhmodik, S.M., Mironov, A.G., Borovikov, A.A., Gold mineralization in siliceous–carbonate rocks of southeastern East Sayan, *Russ. Geol. Geophys.,* 2007, vol. 48, no. 5, pp. 389–399.

Beaudoin, G. and Therrien, P., The web stable isotope fractionation calculator, *Handbook of Stable Isotope Analytical Techniques,* De Groot, P.A., Ed., Elsevier: 2004, vol. 1, pp. 1045–1047.

Beaudoin, G. and Therrien, P., The updated web stable isotope fractionation calculator, *Handbook of Stable Isotope Analytical Techniques,* De Groot, P.A., Ed., Elsevier, 2009, vol. 1, pp. 1120–1122.

Beaudoin, G. and Pitre, D., Stable isotope geochemistry of the Archean Val-d'Or (Canada) orogenic gold vein field, *Mineral. Deposita,* 2005, vol. 40, pp. 59–75.

Bodnar, R.J. and Vityk, M.O., Interpretation of microthermometric data for H_2O–NaCl fluid inclusions, in *Fluid Inclusions in Minerals, Methods and Applications,* B. De Vivo and M. L. Frezzotti, Eds., Blacksburg: Virginia Tech, 1994, pp. 117–130.

Borisenko, A.S., Cryometric study of salt composition of gas–liquid inclusions in minerals, *Geol. Geofiz.,* 1977, no. 8, pp. 16–27.

Buslov, M.M., Tectonics and geodynamics of the Central Asian Foldbelt: the role of late Paleozoic Large-amplitude strike-slip faults, *Russ. Geol. Geofiz.,* 2011, vol. 52, no. 1, pp. 66–90.

Damdinov, B.B., Zhmodik, S.M., Roshchektaev, P.A., et al., Composition and Genesis of the Konevinsky gold deposit, Eastern Sayan, Russia, *Geol. Ore Deposits,* 2016, vol. 58, no. 2, pp. 134–148.

Fedotova, A. A. and Khain, E.V., *Tektonika yuga Vostochnogo Sayana i ego polozhenie v Uralo-Mongol'skom poyase* (Tectonics of the Southern Eastern Sayan and its Position in the Ural–Mongolian Belt*),* Moscow: Nauchnyi mir, 2002.

Faure, G., *Principles of Isotope Geology,* New York: Wiley, 1986.

Gamyanin, G. N., *Mineralogo-geneticheskie aspekty zolotogo orudeneniya Verkhoyano-Kolymskikh mezozoid* (Mineralogical-geochemical Aspects of Gold Mineralization of the Verkhoyansk–Kolyma Mesozoides), Moscow: GEOS, 2001.

Geologiya i rudonosnost' Vostochnogo Sayana (Geology and Ore Potential of Eastern Sayan), Dobretsov, N.L. and Belichenko, V.G., Eds., Novosibirsk: Nauka, 1989.

Gidrotermal'nyi rudogenez okeanskogo dna (Hydrothermal Ore Genesis of Ocean Floor), Bogdanov, Yu.A., Ed., Moscow: Nauka, 2006.

Goldfarb, R.J., Baker, T., Dube, B., Groves, D.I., Hart, C.J.R., and Gosselin, P., Distribution, character and genesis of gold deposits in metamorphic terrains, *Econ. Geol.,* 2005, vol. 100, pp. 407–450.

Gordienko, I.V., Roshchektaev, P.A., and Gorokhovskii, D.V., Oka ore district of the Eastern Sayan: geology, structural–metallogenic zonation, genetic types of ore deposits, their geodynamic formation conditions, and outlook for development, *Geol. Ore Deposits,* 2016. vol. 58, no. 5, pp. 361–382.

Grebenshchikova, V.I. and Shmotov, A.P., Stages of the formation of the Zun-Kholbin gold deposit, Eastern Sayan, *Geol. Geofiz.,* 1997, vol. 38, no. 4, pp. 756–764.

Groves, D.I., Goldfarb, R.J., Gebre-Mariam, M., Hagemann, S.G., and Robert, F., Orogenic gold deposits: a proposed classification in the context of their crustal distribution and relationship to other gold deposit types, *Ore Geol. Rev.,* 1998, vol. 13, pp. 7–27.

Hoefs, J., *Stable Isotope Geochemistry,* 6th Edition, Berlin–Heidelberg: Springer-Verlag, 2009.

Keighin, C.W. and Honey, R.M., The system Ag–Sb–S from 600 to 200°C, *Mineral. Deposita,* 1969, vol. 4, nos. 2, pp. 153–171.

Khain, E.V., Bibikova, E.V., Kroner, A., et al., The most ancient ophiolite of the Central Asian fold belt: U–Pb and Pb–Pb zircon ages for the Dunzhugur complex, Eastern Sayan, Siberia, and geodynamic implications, *Earth Planet. Sci. Lett.,* 2002, vol. 199, pp. 311–325.

Khubanov, V.B., Buyantuev, M.D., and Tsygankov, A.A., U–Pb dating of zircons from PZ_3–MZ igneous complexes of Transbaikalia by sector-field mass spectrometry with laser sampling: technique and comparison with SHRIMP, *Russ. Geol. Geophys.,* 2016, vol. 57, no. 1, pp. 190–205.

Kirgintsev, A.N., Trushnikova, L.N., and Lavrent'eva, V.G., *Rastvorimost' neorganicheskikh veshchestv v vode. Spravochnik* (Solubility of Inorganic Matters in Water. A Textbook), Leningrad: Khimiya, 1972.

Kuzmichev, A.B., *Tektonicheskaya istoriya Tuvino-Mongol'skogo massiva: rannebaikal'skii, pozdnebaikal'skii i rannekaledonskii etapy* (Tectonic Evolution of the Tuva–Mongolian Massif: Early Baikalian, Late Baikalian, and Early Caledonian), Moscow: Probel-2000, 2004.

Kuzmichev, A.B. and Larionov, A.N., Neoproterozoic island arcs in East Sayan: duration of magmatism (from U–Pb zircon dating of volcanic clasts), *Russ. Geol. Geophys.,* 2013, vol. 54, no. 1, pp. 34–43.

Li, Y. and Liu, J., Calculation of sulfur isotope fractionation in sulfides, *Geochim. Cosmochim. Acta,* 2006, vol. 70, pp. 1789–1795.

Mironov, A.G. and Zhmodik, S.M., Gold Deposits of the Urik–Kitoi Metallogenic Zone (Eastern Sayan, Russia), *Geol. Ore Deposits,* 1999, vol. 41, no. 1, pp. 46–60.

Mironov, A.G., Bakhtina, O.T., Zhmodik, S.M., et al., A new type of gold mineralization in stratiform pyrrhotite ores in the Eastern Sayan Range, *Dokl. Earth Sci.,* 1999, vol. 365, pp. 337–340.

Mironov, A.G., Zhmodik, S.M., Ochirov, Yu.Ch., et al., The Tainskoe gold deposit (Eastern Sayan, Russia)–a new example of the porphyry gold type, *Geol. Ore Deposits,* 2001, vol. 43, no. 5, pp. 353–370.

Mironov, A.G., Zhmodik, S.M., Ochirov, Yu.Ch., et al., Geochemistry and metal potential of the carbonaceous rocks of different geodynamic settings of the Sayan–Baikal fold system, *Geol. Geofiz.,* 2002, vol. 43, nos. 3–4, pp. 348–365.

Ohmoto, H. and Rye, R.O., Isotopes of sulfur and carbon, in *Geochemistry of Hydrothermal Ore Deposits,* 2nd edition, Barnes, H.L. Ed., New York: J. Wiley and Sons, 1979, pp. 461–560.

Petrovskaya, N.V., *Samorodnoe zoloto (obshchaya kharakteristika, tipomorfizm, voprosy genezisa)* (Native Gold: General Characteristics, Typomorphism, and Genetic Problems), Moscow: Nauka, 1973.

Phillips, J.N. and Powell, R., Formation of gold deposits: a metamorphic devolatilization model, *J. Metamorph. Geol,* 2010, vol. 28, pp. 689–718.

Ridley, J.R. and Diamond, L.W., Fluid chemistry of orogenic lode gold deposits and implications for genetic models, *SEG Rev.,* 2000, vol. 13, pp. 141–162.

Seal, R.R., Sulfur isotope geochemistry of sulfide minerals, *Rev. Mineral. Geochem,* 2006, vol. 61, pp. 633–677.

Travin, A.V., Yudin, D.S., Vladimirov, A.G., et al., Thermochronology of the Chernorud granulite zone, Ol'khon Region, western Baikal Area, *Geochem. Int.,* 2009, vol. 47, no. 11, pp. 1107–1124.

Zhang, L.-G., Liu, J.-X., Zhou, H.B., and Chen, Z.-S., Oxygen isotope fractionation in the quartz–water–salt system, *Econ. Geol.,* 1989, vol. 89, pp. 1643–1650.

Zhmodik, S.M., Mironov, A.G., and Zhmodik, A.S., *Zolotokontsentriruyushchie sistemy ofiolitovykh poyasov (na primere Sayano-Baikalo-Muiskogo poyasa)* (Gold-Concentrating Systems of Ophiolite Belts by the Example of the Sayan–Baikal–Muya Belt), Novosibirsk: "Geo", 2008.

Zhmodik, S.M., Postnikov, A.A., Buslov, M.M., et al., Geodynamics of the Sayan–Baikal–Muya accretion–collision belt in the Neoproterozoic–Early Paleozoic and regularities of the formation and localization of precious-metal mineralization, *Russ. Geol. Geophys.,* 2006, vol. 47, no. 1, pp. 187–201.

Znamenskii, S.E. and Znamenskaya, N.M., Ore-hosting transtensive duplexes of gold–quartz and gold–sulfide–quartz deposits of the South Urals, *Litosfera,* 2011, no. 1, pp. 94–105.

Zoloto Buryatii. Kn. 1. Strukturno-metallogenicheskoe raionirovanie, geologicheskoe stroenie mestorozhdenii, resursnaya otsenka (Gold of Buryatia. Book 1. Structural-Metallogenic Zoning, Geological Structure of Deposits, and Resource Assessment), Roshchektaev, P.A., Mironov, A.G., Doroshkevich, G.I., et al., Eds., Ulan-Ude: BNTs SO RAN, 2000.

Translated by V. Popov